The *Drosophila* proventriculus lacks stem cells but compensates for age-related cell loss via endoreplication-mediated cell growth

Authors: Ben Ewen-Campen[1*], Weihang Chen[1], Sudhir Gopal Tattikota[1], Ying Liu[1], Yanhui Hu[1], Norbert Perrimon[1,2*]

Affiliations:

1. Department of Genetics, Blavatnik Institute, Harvard Medical School, Boston, MA 02115, USA
2. Howard Hughes Medical Institute, Boston, MA 02115, USA

***Corresponding author**: Ben Ewen-Campen and Norbert Perrimon
Email: bewencampen@genetics.med.harvard.edu, perrimon@genetics.med.harvard.edu

Abstract

The *Drosophila* proventriculus is a bulb-shaped structure at the juncture of the foregut and the midgut, which plays important roles in ingestion, peritrophic membrane synthesis, and the immune response to oral pathogens. A previous study identified a population of cells in the proventriculus which incorporate bromodeoxyuridine (BrdU), a marker of DNA synthesis, and proposed that these cycling cells are multipotent stem cells that replace dying cells elsewhere in the tissue. Here, we re-investigate these cycling cells and find that they do not undergo mitosis, do not generate clonal lineages, and do not proliferate in response to tissue damage, and are therefore not stem cells. Instead, we find that these cells continually endocycle throughout the fly's life, increasing their ploidy and size, while at the same time cells in this tissue are lost into the gut lumen as the fly ages. Functionally, these cells play a critical role in the synthesis of peritrophic membrane components, and we show that when endocycling in these cells is experimentally increased or decreased, there is a concomitant change in ploidy, tissue size, and peritrophic membrane synthesis. Further, we show that inhibition of endocycling makes flies more susceptible to orally infectious bacteria. Altogether, we show that continual endocycling of these cells is critical for maintaining tissue size and function in the face of cell loss due to aging or tissue damage.

Introduction

The *Drosophila* gut is a highly regionalized organ with distinct functional domains along its length[1–3]. Within each domain, in addition to primary roles such as nutrient absorption and immunity, there are cellular mechanisms to ensure that the gut is repaired and renewed following tissue damage or cell loss. In the midgut, there are multipotent intestinal stem cells (ISCs) that continually divide to replace the differentiated cell types of the gut, both during homeostasis[4,5] and in response to tissue damage[6,7]. Analogous ISCs are present in the mammalian small intestine[8,9], which is functionally comparable to the *Drosophila* midgut[10].

In contrast to the midgut, in the hindgut there is no evidence of multipotent stem cells[11,12]. Instead, hindgut cells respond to tissue damage by undergoing extensive endocycling, a specialized cell cycle in which DNA is replicated without undergoing mitosis, thus increasing the ploidy and nuclear size of hindgut cells [11] . In *Drosophila*, this endocycling response to tissue damage or wounding is conserved in the adult epidermis [11,13,14] , and is important to maintain tissue integrity in the absence of stem cell activity.

At the anterior of the gut, where the foregut meets the midgut, there is a specialized bulb-shaped structure called the proventriculus (also known as the cardia, based on its shape). A previous study[15] identified a ring of cells in the proventriculus which incorporate the nucleotide analog BrdU, a marker of S phase, and proposed that these cycling cells are stem cells that replace dying cells elsewhere in the proventriculus.

Here, we re-investigate the function of these previously identified cycling cells in the proventriculus. We find no evidence that these cells undergo mitosis, generate clonal lineages,

or proliferate in response to tissue damage in other regions of the proventriculus. Instead, we find that these cells continually endocycle throughout the fly's life, at a rate that varies with systemic nutritional signals. Further, we find that cells from this region of the proventriculus are progressively lost into the gut lumen as the fly ages, and that this cell loss drives nearby cells to endocycle and thereby increase in ploidy and size. Lastly, we show that blocking endocycling in these cells reduces peritrophic membrane synthesis, whereas inappropriately enhancing endocycling leads to increased peritrophic membrane synthesis. We conclude that the proventriculus does not contain stem cells, but that it instead compensates for age-related cell loss by endocycling-mediated cell growth to maintain tissue function.

Results and Discussion

A ring of cycling cells in Zone 4. The proventriculus consists of a doubly-folded tubular epithelium and associated muscles and neuronal structures (Figure 1A)[16–18] . It forms during embryogenesis by the invagination of an anterior, ectodermal portion of the embryonic gut (the future esophagus) into an adjacent segment of endodermal gut, creating a bulb structure with an internal lumen[19–21] . In addition to serving as a muscular valve surrounding the esophagus, the proventriculus plays a critical role in the synthesis of the peritrophic membrane, a chitin- and mucin-rich structure that lines the midgut[16–18] . Studies in other Dipterans have shown that the proventriculus is capable of producing peritrophic membrane at a rate exceeding six mm/hour at 25ºC, representing an enormous capacity for synthesis and secretion[22,23]. In addition to peritrophic membrane synthesis, the proventriculus plays important roles in the immune system [24,25] , and as a site for regulation of the microbiota[26] .

Morphological studies have identified six distinct "zones" arranged linearly along the proventriculus epithelium, based upon cellular morphology and on their proposed role in the synthesis of the peritrophic membrane[16]. These anatomical zones have been shown via single cell RNAseq (scRNAseq) to correspond to transcriptionally distinct cell types[25].

Zone 4 is a ring-shaped structure that encircles the esophagus at the anterior of the proventriculus (Figure 1A). A previous study identified a ring of cells located at the posterior limit of Zone 4 which consistently incorporate BrdU, indicating that these cycles progress through S phase in adult flies[15]. This study proposed that these cycling cells are multipotent stem cells that proliferate and replace dying cells elsewhere in the proventriculus[15]. An alternative hypothesis, not explored by Singh *et al.*[15], is that these cells are endocycling and thus undergoing repeated S phases without mitosis.

Functionally, Zone 4 cells are highly secretory and play an important role in the synthesis of chitin and other peritrophic membrane components[16,25,27]. scRNAseq studies indicate it is enriched for genes involved in chitin synthesis and chitin modifications, including *chitin synthase 2 (Chs2)*[25] which can be visualized with *Chs2-Gal4 > UAS:2XEGFP* (Figure 1B, left). Studies in larval flies confirm that mutations in *Chs2* lead to defects in peritrophic membrane synthesis[27], and visualizing the peritrophic membrane with fluorescently labeled Helix pomatia (HPA) lectin[28,29] confirms previous observations that peritrophic membrane components is highly

enriched in the lumen directly abutting Zone 4 cells (Figure 1B, middle.) Zone 4 cells also express high levels of the WNT pathway ligand Wingless (Figure 1C, right), as previously reported[15].

To re-investigate the function of these cycling cells, we fed flies with EdU for two days and confirmed the presence of a ring of EdU+ cells at the posterior edge of Zone 4 (Figure 1C, left). EdU+ cells are occasionally observed elsewhere in the proventriculus (see e.g. Figure 1F, 2A), but here we focus exclusively on the EdU+ population in Zone 4. Previous studies suggested that, in addition to Wg expression, JAK-STAT signaling is also enriched in this area[15], and when we co-labeled proventriculi for EdU and *10XSTAT:GFP*, a JAK-STAT pathway reporter, we found that the EdU+ population is directly anterior to STAT+ cells, suggesting that EdU+ cells are enriched at the posterior edge of Zone 4, with *10XSTAT:GFP* expression representing the anterior limit of Zone 3 (Figure 1C, right).

To characterize the dynamics of EdU incorporation over time, we fed flies with EdU for 1, 3, or 5 days. We performed this experiment with two standard lab genotypes, w^{1118} and *OreR,* and observed that the number of labeled cells increased linearly with time (Figure 1D,E; simple linear regression, $p < 0.0001$ that slope is non-zero for both genotypes) at a rate of between 3.3 (w^{1118}) and 4.1 (*OreR*) EdU+ cells per day, suggesting that cells in this region are continually entering S phase at a relatively constant rate. The number of EdU+ cells detected for these two genotypes were not significantly from one another at each time point (Figure 1E).

To test whether individual cells cycle continuously over time or whether they cease cycling after a discrete number of S phases, we performed a pulse-chase experiment by feeding EdU for 3 days, followed by a 20 day chase in the absence of EdU (Supplementary Figure 1). After 20 days, we observed significantly fewer in EdU+ cells in Zone 4, suggesting that the EdU signal was diluted by continued cycling (Supplementary Figure 1). This dilution over time is similar to what is observed for the continually cycling ISCs, in which EdU labeling is diluted through mitosis, and in enterocytes (ECs), which endocycle and thereby dilute the proportion of Edu-labeled DNA in each nucleus over time (Supplementary Figure 1). In contrast, these results differ from what is observed in the hindgut, where BrdU signal is retained for 20 days due to a lack of continual cycling under homeostasis[11].

It has previously been shown that systemic nutritional signals tightly correlate with endocycle progression in a variety of cellular contexts in the *Drosophila* larva, whereas mitotic activity is not clearly linked to nutritional status[30,31]. We tested whether the EdU+ cells in Zone 4 are responsive to nutrition by varying the amount of dry active yeast, a primary source of protein and other macronutrients for *Drosophila*, added to a standard minimal lab food. We found that the number of EdU+ cells steadily increased in response to additional yeast added to the fly's food (Figure 1F-G; one-phase association model, rate constant K = 0.5689 [95% CI = 0.1639 to 1.463]), suggesting that the cycling of these cells is influenced by systemic nutritional cues.

We further tested this sensitivity to systemic nutrition using a genetic tumor model in the midgut (*esg-Gal4, tubGal80^{ts} > UAS:yki^{3SA};* note that *esg-Gal4* is not expressed in the proventriculus), which promotes systemic muscle wasting and cachexia via the upregulation of the systemic insulin antagonist *Impl2,* the cytokine *upd3,* and other cytokines[32–34]. In cachectic flies, we observed a significant decrease in the number of EdU+ cells in the proventriuclus (Supplementary Figure 2A,B), suggesting that cycling in these cells responds to systemic insulin signaling. We then tested whether over-expressing the insulin antagonists *Impl2, upd3*, or both together, would lead to a similar reduction in EdU+ cells in the proventriculus. Indeed, when we expressed these factors from ISCs using *esg-Gal4*, we observed a significant decrease in EdU+ cells of the proventriculus (Supplementary Figure 2C). Previous studies have shown that, in addition to ISCs, *esg-Gal4* is also expressed in the corpus allatum, located near the proventriculus. We thus used an independent Gal4, *dMef2-Gal4*, to over-express secreted factors from the muscles, and observed a significant decrease in EdU+ cells in the proventriculus (Supplementary Figure 2D).

Altogether, these observations confirm that the adult proventriculus contains a ring of cells at the posterior of Zone 4 which consistently cycle through S phase, and that they do so in response to systemic nutritional signals.

Single nucleus atlas and Gal4 toolkit for the proventriculus. In order to functionally characterize these EdU+ cells *in vivo*, we generated a toolkit of Gal4 lines to label and manipulate various cell types of the proventriculus, building on a recent single cell atlas generated for this tissue[25]. First, we screened the K-Gut database[35] for Gal4 lines that specifically label Zone 4. We identified four lines that labeled Zone 4, inclusive of EdU+ cells, (*GMR41F06-GAL4, GMR26D04-GAL4, GMR56D02-GAL4, and GMR71F06-Gal4*) and selected a particularly specific and consistent line, *71F06-Gal4*, for further study (Figure 2A).

Next, to identify molecular markers for other proventriculus cell types and to serve as a foundation for further molecular study, we created a single cell transcriptional atlas of the proventriculus using single nucleus RNAseq (snRNAseq). We sequenced a total of 22,332 nuclei from approximately 600 dissected proventriculus tissues, which ultimately resolved into 14 transcriptionally-defined clusters (Figure 2B,C,D). This atlas is available via an online data portal (https://www.flyrnai.org/scRNA/proventriculus/).

We mapped the identity of these snRNAseq clusters to *in vivo* anatomy using cluster-specific marker genes. One cluster was enriched for molecular markers of muscles (e.g. *Mhc, up*) and two clusters were enriched for pan-neuronal markers (e.g. *nSyb, elav, brp*), one of which was enriched for *Akh*- and *Impl2*-expressing cells and therefore likely represents the corpora cardiaca[36–38]. To map the remaining 11 clusters to the *in vivo* proventriculus, we examined the expression of top marker genes for each cluster using either Gal4 lines or split-intein Gal4 lines crossed to a ubiquitous reporter (Figure 2C,D,E.)[39].

We were able to identify the remaining clusters as anatomically distinguished epithelial cell types. One cluster corresponded to the esophagus (marked by *Elovl7-Gal4*), another to Zone 1

(marked by *CG11550-Gal4* and *Cht7-Gal4*). At the clustering resolution we selected, Zone 2 and 3 cells were both found in a single cluster (enriched for *Ppn-Gal4* and *Cyp49a1-Gal4*). We observed a distinct cluster enriched for *Lgr1* and *Delta* that corresponds to a population of cells specifically at the anterior border of Zone 3, immediately posterior to Zone 4. We recovered distinct clusters corresponding to Zone 4 (*Wnt4-Gal4*) and Zone 5 (*Ca-Ma2d-Gal4*), as well as a cluster that corresponds to a discrete band of cells at the widest diameter of the proventriculus, at the border of Zone 5 and 6 (marked by *CG10702-Gal4, Notum-Gal4*, *Mco4-Gal4*$^{N\text{-}int}$). A cluster enriched for *SecCl-Gal4* corresponded to Zone 6, and a cluster enriched *mex1-Gal4* and *P5CS-Gal4* corresponded to the anterior midgut. Two additional minor clusters (labeled "unknown" and "anterior midgut 1" in Figure 2B) were enriched for markers corresponding to multiple cell types and were excluded from further analysis.

We queried our atlas for markers of stem cells. In a previous scRNAseq atlas of the *Drosophila* midgut[40], midgut ISC clusters were enriched for the stem cell marker *esg*, as well as cell-cycle related genes *PCNA* and *stg.* We did not observe notable expression of any of these genes, nor any cluster-specific enrichment for any *Cyclin* genes, in our proventriculus atlas, whether in our Zone 4 cluster or elsewhere.

Our snRNAseq atlas is largely concordant with a recently published scRNAseq atlas of the proventriculus[25], with minor deviations in the proportions of cells present in each cluster (Supplementary Figure 3). This high degree of concordance suggests that the cell types we identify are robust to experimental approach, as these two atlases were created using entirely different single cell protols; Zhu (2024) sequenced single cells from freshly dissected and chemically dissociated suspensions, while we sequenced isolated nuclei from flash frozen tissues. We also note that our atlas was generated from two biological samples: proventriculi from control flies and from cachectic flies, and thus includes cells across a range of nutritional status (see Methods). This snRNAseq atlas thus serves as a resource for studies of the proventriculus, and allows us to identify cell type-specific Gal4 driver lines for functional experiments.

No evidence for mitosis in the proventriculus. Stem cells are defined as multipotent precursor cells that undergo repeated asymmetric mitosis, giving rise to one daughter cell that retains a stem identity and another daughter cell capable of differentiation. Thus, mitosis is a critical feature of any stem cell system. A previous study of the proventriculus suggested that rare mitoses do occur in this tissue, albeit at a rate that is seemingly out of proportion with the steady numbers of cells passing through S phase[15].

To re-examine whether these cells undergo mitosis, we first stained guts from two different control genotypes (20 *OreR* wildtype guts, 36 *71F06-Gal4 > UAS:2XEGFP* guts, total n = 56 guts) for phosphorylated Histone 3 (pH3+), a marker of mitosis. We fed these flies colchicine overnight prior to staining, which enriches for pH3+ cells by blocking exit from mitosis[11]. We observed zero pH3+ cells in the epithelia of Zone 4 in these flies, or anywhere else in the proventriculus.

The cell cycle can be experimentally driven forward using a variety of genetic manipulations, and in cells that are capable of mitosis these manipulations will dramatically increase M phase. For example, in ISCs of the posterior midgut, over-expression of *UAS-yki*^{3SA}[41–43] or *UAS-Ras*^{1A}[44–46], or *Notch-RNAi*[4,5] all lead to dramatic increases in mitosis, leading to massive tumor growth. We hypothesized that, if Zone 4 cells are competent to undergo mitosis, over-expression of such cell cycle promoting factors should lead to an increase in mitotic cells.

To test whether these factors can drive mitotic proliferation in the proventriculus, we used *71F06-Gal4*^{ts} to drive *UAS-yki*^{3SA}, *UAS-Ras1*^{A}, or *Notch-RNAi* in Zone 4 cells, and then stained for pH3 as a marker of mitosis following enrichment via colchicine (here and below, *71F06-Gal4*^{TS} refers to flies containing both the *71F06-Gal4* driver and *tubGal80*^{ts}, to restrict Gal4 function to adult flies.)

All of these genetic manipulations led to significant increases in the number of EdU+ cells and the size of Zone 4 measured as the cross-sectional area at the tissue's widest point (Figure 3 and S4A-D, S4F-H). Under these staining conditions, we could detect over 600 mitotic ISCs in the midgut that stained positively for pH3 (Figure 3B). In contrast, we did not observe a single pH3+ cell in the proventriculus under any of these conditions (Figure 3B). Interestingly, however, we did observe a significant increase in the ploidy of Zone 4 nuclei following over-expression of both *UAS-yki*^{3SA} and *UAS-Ras1*^{A}, indicating that these manipulations promote endocycling (Supplementary Figure 4E and see below.) In contrast, while *Notch-RNAi* did increase the number of EdU+ cells, it did not increase ploidy, suggesting *Notch* signaling in the proventriculus may function to restrict inappropriate entry into S phase and/or endocycle progression, but not completion of the endocycle.

These results demonstrate that EdU+ cells located in Zone 4 of the proventriculus do not undergo mitosis either under homeostatic conditions or when experimentally driven through cell cycle progression via ectopic oncogene expression. Furthermore, we note that despite morphological deformities caused by over-expressing activated Yki or Ras1, we never saw GFP+ cells located outside of Zone 4, which provides further evidence that cycling cells in Zone 4 do not migrate to replace damaged or dead cells in other regions of the tissue as suggested by Singh *et al.*[15].

No evidence for clonal growth of Zone 4 cells. Despite the absence of pH3 staining, it is formally possible that rare mitoses occur. Another hallmark of adult stem cells is the ability to generate multipotent clones in the adult organism. For example, in the adult posterior midgut, *MARCM*-based lineage tracing of ISCs leads to the presence of GFP-labeled clones throughout the midgut that contain all of the epithelial cell types that can be generated by ISC differentiation[4,5]. We therefore used *MARCM*-based lineage tracing to test whether there is clonal growth in the adult proventriculus.

As a positive control for our labeling protocol, we heat-shocked *MARCM* larvae during the L3 larval stage, when this tissue is still undergoing developmental proliferation. We observed large GFP+ clones throughout the proventriculus, both in Zone 4 and elsewhere, in every sample

examined, demonstrating that *MARCM* labeling functions as expected in this tissue (Figure 4A). As a negative control, we examined GFP+ patterns in both midguts and proventriculi from non heat-shocked flies, and observed small numbers of scattered GFP+ cells throughout the proventriculus, as well as in the midgut. We scored proventriculi as having either no GFP+ clones, between 1-5 small groups of GFP+ cells (typically 1-2 cells each), or having large GFP+ clones that include >10 cells (Figure 4D).

To test for clonal growth during the adult stage, we heat-shocked *MARCM* flies several days after eclosion, then reared them for varying lengths of time before scoring for GFP+ clones. We challenged an additional cohort of flies with a 2-day starvation followed by re-feeding, which increases ISC proliferation in the midgut[47,48].

As expected, in the posterior midgut we observed GFP+ clones in the midguts of heat-shocked flies after 14 days, and we also found that these clones tended to be larger in flies that experienced a 2 day starvation (Figure 4B). In contrast, in the proventriculus of these flies, we observed scattered singlet and doublet GFP+ cells throughout the tissue at roughly similar rates between negative controls and heat-shocked flies (Figure 4C,D). This was true at 14 days after heat-shock, 19 days after heat-shock, and 30 days at 18ºC after heat-shock (Figure 4C,D). We did observe a single example of a large clone in one cohort of heat-shocked animals (Figure 4D), which was likely a rare example of a *MARCM* clone being formed via leaky FLP expression during earlier development.

In the midgut, ISCs divisions increase dramatically upon tissue damage[6,7]. To test whether there may be damage-responsive proliferation in the proventriculus, we repeated these *MARCM* experiments in flies subjected to a variety of gut damage conditions: bleomycin treatment, infection with pathogenic *ECC15* bacteria, and 2000 RADs of X-rays[6,7]. We also performed *MARCM* experiments with 10% yeast supplementation because we had observed that EdU incorporation rates increased with yeast supplementation. We did not observe discernable GFP+ clones emanating from Zone 4 or any other area of the proventriculus in any of these conditions (Supplementary Figure 5). We note the caveat that, unlike enterocytes of the midgut, Zone 4 cells do not directly contact the contents gut lumen and therefore likely do not experience the same degree of damage that ECs experience in contact with bleomycin or *ECC15*. Nonetheless, we did not observe GFP+ clonal growth under any of these conditions. Altogether, we find no evidence for clonal growth of the EdU+ cells in Zone 4 of the proventriculus.

No proliferation in response to distant tissue damage. Singh *et al*. proposed that the EdU+ cells in the proventriculus are proliferating for the purpose of migrating to replace dying cells elsewhere in the tissue[15]. This hypothesis implies that cells originating in Zone 4 proliferate in response to cell death in nearby tissues, and then migrate to such nearby tissues as the esophagus, anterior midgut, and crop.

To directly test how the EdU+ cells of Zone 4 respond to cell death in nearby tissues, we used the Gal4-UAS system to induce cell death in various regions of the proventriculus by over-

expressing the proapoptotic factor *UAS-rpr*. We induced cell death in three different cell types of the proventriculus: in Zone 5 (*Ca-Ma2d-Gal4*), in Zone 1 (*CG11550-Gal4*), and in the esophagus (*Evolv7-Gal4*) (Figure 4). In these experiments, we silenced *UAS-rpr* throughout development using *tubGal80*^{ts} and raised flies at 18ºC until several days post-eclosion. We activated tissue damage by shifting adult flies to 29ºC for 48 hours, and placed flies on EdU-containing food for the duration of the tissue damage, and throughout a recovery phase of 2 days or 5 days at 18ºC following damage. If these EdU+ cells in Zone 4 proliferate to compensate for dying cells, we would expect to see an increase in EdU+ cells in response to damage in neighboring cells, and likely EdU+ cells migrating towards the area of damage.

In all three experiments, we observed pyknotic nuclei, indicative of apoptosis, in the intended cell type in *UAS-rpr* flies, and not in control flies (Figure 5A,B,C), indicating that this system induces apoptosis as expected. However, in all three experiments we observed not an increase in EdU+ cells, but rather a significant decrease (Figure 5.) These results are inconsistent with the hypothesis that these cells proliferate in response to tissue damage elsewhere in the proventriculus. The decrease in EdU+ cells supports our previous observation that these cells cycle in response to cues indicative of organismal health.

Interestingly, when we drove apoptosis in the esophagus with *Elovl7-Gal4*, while we observed a decrease in EdU+ cells in Zone 4, we did observe indications of massive endoreplication in the esophagus itself: unusually large, EdU+ nuclei (Figure 5C, asterisks). This is similar to what has been reported in the hindgut[11]. In contrast, tissue damage to Zone 1 or Zone 5 did not cause an obvious increase in endoreplication in the damaged tissue (Figure 5A,B).

Genetic lineage tracing of EdU+ cells in Zone 4. As a final test for lineage tracing independent of MARCM, we wished to genetically label the descendants of Zone 4 EdU+ cells using a Gal4 line specific to these cycling cells. However, we did not observe any discernible transcriptional signatures of the Zone 4 EdU+ cells, and were initially unable to identify a Gal4 driver to specifically label these cells within Zone 4.

We thus used the split-intein Gal4 system to generate a genetic driver that specifically labels the EdU+ population of cells in Zone 4[39]. We generated a split-intein Gal4$^{N\text{-}int}$ line using the 71F06 enhancer fragment (Supplementary Figure 6A; referred to here as *71F06*$^{Gal4\text{-}C\text{-}int}$), and then used our snRNAseq atlas to identify *Delta* as a candidate gene which is primarily enriched in Zones 1-3 and in Zone 3-4 border cells, with some expression as well in Zone 4 (Supplementary Figure 6A). When we examined the intersectional labeling of *71F06*$^{Gal4\text{-}C\text{-}int}$ *∩ Delta*$^{Gal4\text{-}N\text{-}int}$ > *UAS:2xEGFP*, we observed specific expression in a band of cells at the posterior edge of Zone 4 (Supplementary Figure 6A). We confirmed that these cells contain the large majority of EdU+ cells (Supplementary Figure 6A).

To lineage trace these cells, we used the G-TRACE system combined with *tubGal80*^{ts}, which labels current expression in RFP and lineage expression in GFP[49]. After development at 18ºC, we placed *71F06*$^{Gal4\text{-}C\text{-}int}$ *∩ Delta*$^{Gal4\text{-}N\text{-}int}$*, tubGal80*^{ts} > *G-TRACE* at 29ºC to initiate lineage

tracing and examined the proventriculus after 1 day, 6 days at 10 days (Figure 6C,D). If these cells are proliferating and generating clones, we would expect to see progressively more GFP+ / RFP- cells, as descendants of these cells would grow into the rest of the tissue. However, while we did observe small numbers of GFP+ / RFP- cells immediately adjacent to the GFP+/RFP+ domain, the number of these cells did not increase or move over time, but were constant over a 10 day period (Figure 6C,D). These results are consistent with leaky and/or minor dynamic changes in the expression pattern of our split-intein Gal4 line, rather than with proliferation of cells in this domain.

Taken together, we find no evidence that the EdU+ cells located in Zone 4 are stem cells. We do not observe mitosis, nor the generation of MARCM clones, nor a proliferative response to nearby tissue damage, nor any evidence of genetic cell lineages growing over time. We thus propose that these cells must be endocycling rather than undergoing mitosis.

Cells in Zone 4 increase in ploidy as flies age. The consistency with which EdU is incorporated into cells in Zone 4 suggests that these cells are continually endocycling throughout the fly's life, which should lead to increased ploidy as flies age. To test this directly, we performed a time-course experiment using confocal microscopy to quantify the ploidy of Zone 4 nuclei over the course of fly aging. In this experiment, *71F06-Gal4* > *UAS:GFP*^{stinger} flies (hereafter, *UAS:GFP*^{NUC}), which express nuclear-localized GFP in Zone 4, were split into vials either containing dried active yeast powder *ad libitum* or standard food lacking additional yeast powder, and were examined at six timepoints between 3 days and 35 days after eclosion. At each time-point, we collected 5 confocal z-stacks and quantified the ploidy and the volume of these nuclei (Supplementary Figure 7).

We observed a consistent increase in ploidy and nuclear volume over the course of the fly's life, supporting the hypothesis that these cells are continually endocycling and increasing in ploidy (Figure 6A,B,C and S7A,B; relationship between age and ploidy was significantly different than zero; simple linear regression; n = 960/1064 cells[no yeast/yeast], $p < 0.0001$ for both no yeast and yeast).

Consistent with the observation that supplemental yeast increases EdU incorporation, we found that the 7d and 14d timepoints, ploidy was significantly higher in flies which received dried active yeast, but that by 21 days the average ploidy was not significantly different between these treatments (Figure 6A,B,C). Over this time-course, the mean ploidy of Zone 4 cells increased from ~4C at 3 days (2.1-2.2 x diploid, with or without yeast) to ~10C at 35 days (4.8-4.9 x diploid), while the maximum ploidy amongst Zone 4 cells increased from ~9C (4.3-4.6 x diploid) to ~22-26C (11.1-13.0 x diploid) between these time points. We found no evidence that Zone 4 cells become multinucleate, based on co-staining these samples with the f-actin marker, even at the latest time point (35d) when the tissue begins to lose a clearly monolayered structure (Supplementary Figure 6C).

Zone 4 cells are progressively lost into the gut lumen. Surprisingly, we observed that while the volume of Zone 4 nuclei progressively increased, the total number of GFP+ nuclei steadily

decreased (Figure 6D). Over the first 14 days, cell numbers decreased at equivalent rates for flies fed with or without yeast, but beginning at 21 days the number fell faster for flies without added yeast (Figure 6D). Remarkably, we could observe “snap shots” of this cell loss in fixed samples, visible as GFP+ nuclei being shed into the gut lumen at the time of dissection (Figure 6E and S7). We quantified the number of GFP+ nuclei present in the lumen outside the Zone 4 epithelium in these fixed tissues and found that the number of GFP+ cells outside of Zone 4 first started to increase at 14 days after eclosion, and subsequently increased until reaching a maximum at 28 days (Figure 6F). We did not observe any obvious morphological differences in the cells being lost, and the mechanism by which these cells exit the epithelium is not known, but we observed holes forming in the F-actin-rich barrier separating Zone 4 cells from the gut lumen, with GFP+ nuclei passing through these holes into the lumen (Supplementary Figure 8). We note that the patterns of cell loss neatly with our total cell counts, with the greatest decreases in cell numbers corresponding to those time-points when more nuclei were being lost.

Together, these data suggest that Zone 4 nuclei are endocycling and thus increasing in ploidy and nuclear volume while cells from this region are being lost into the lumen. A simple explanation for these observations is that ploidy is increasing to maintain metabolic output and tissue integrity as cells are progressively lost during aging.

Tissue damage within Zone 4 leads to endocycling. Given our observation that Zone 4 cells endocycle at the same that cells are being lost from the tissue, a simple hypothesis is that endocycling is triggered by the loss of cells from Zone 4, as a compensatory measure. Alternatively, the opposite could be true: as endocycling increases tissue size, this increased tissue size drives the loss of cells to maintain tissue size.

To distinguish between these possibilities, we returned to the genetic cell ablation strategy described above, this time focusing on Zone 4 itself. We raised *71F06-Gal4^{ts} > rpr* and control flies (*71F06-Gal4^{ts}* > +; Figure 7A) at 18ºC until 2-3 days post-eclosion, then shifted them to 29ºC for either 2 or 5 days to induce cell death in Zone 4. During this damage period, flies were fed with EdU-containing food to monitor cell cycling in response to tissue damage. We observed small, pycnotic nuclei throughout Zone 4, indicative of cells in Zone 4 (Figure 7B, arrowheads.)

After 2 days of *rpr* expression in Zone 4 the number of EdU+ cells decreased significantly compared to control flies, but after five days this number had rebounded to control levels (Figure 7C). Notably, the ploidy of these EdU+ cells following five days of tissue damage was significantly increased (Figure 7D). Thus, when cell loss is ectopically induced in Zone 4 via tissue injury, the remaining cells in the tissue endocycle to increase their ploidy. These results are consistent with the hypothesis that Zone 4 cells detect the loss of nearby cells and increase their ploidy via the endocycle in response.

These results indicate that Zone 4 cells can endocycle in response to exogenous damage, yet our previous observations suggest that cells in this tissue also endocycle continuously throughout the fly’s life even in the absence of exogenous damage (Figure 1, Figure 7).

Specifically, we observe continuous endocycling during the first two weeks of the fly's life when there is only a modest amount of cell loss (Figure 7D). To reconcile these observations, we hypothesized that there are two phases of endocycling in this tissue: first, in young flies, endocycling occurs in the absence of cell loss, and is spatially restricted to the posterior edge of the tissue. Subsequently, when naturally occurring cell loss from Zone 4 begins to accelerate in ~2-3 week old flies, a second phase of endocycling begins in response to cell loss, and is spatially distributed throughout Zone 4, in areas nearby the sites of cell loss.

A prediction of this hypothesis is that the spatial distribution of EdU+ cells should be markedly different in the proventriculi of young vs old flies: restricted to the posterior in young flies, and distributed throughout the tissue in older flies. To test this, we collected *OreR* flies at five timepoints between 4d and 31d old, and measured the spatial distribution of EdU+ cells relative to the posterior edge of Zone 4. Remarkably, in younger flies (4d and 11d), EdU+ cells were almost entirely restricted to 1-2 cell diameters from posterior of the tissue (Figure 7E,F). However, in all three of the older time-points (18d, 25d, 31d), in addition to those EdU+ cells located at the posterior of the tissue, there were also many EdU+ cells scattered throughout Zone 4, and these distributions were significantly different from the younger time-points (Figure 7E,F). These results suggest that, in wildtype files under unperturbed conditions, there are two distinct phases of endocycling in the proventriculus: a steady, continuous endocycling in younger flies at the posterior of the tissue, and subsequently throughout the tissue in response to increased cell loss as the fly ages.

Excess endocycling increases peritrophic membrane synthesis. Increasing genomic copy number is a widespread mechanism to enhance synthesis of proteins and other biological components in non-proliferative tissues[31,50,51]. Given the role that Zone 4 cells play in the synthesis and secretion of chitin and other peritrophic membrane components[25,27], we hypothesized that endocycling in this tissue is linked to peritrophic membrane synthesis. We therefore used genetic manipulations to both increase and decrease endocycling and then visualized the peritrophic membrane and tested for functional defects.

To increase endocycling, we overexpressed the cell cycle regulators *UAS:CycE* or *UAS:Myc* in Zone 4 cells using *71F06-Gal4^{ts}*. CycE is a key regulator of both endocycling and the mitotic cell cycle, and drives entry into S phase[31,52], and Myc is a transcription factor whose overexpression is sufficient to drive endocycling and increased nuclear volume in multiple contexts[31,51,53,54]. In Zone 4 cells, both manipulations led to significantly enlarged nuclei after 7-9 days at 29ºC (Figure 8A,B), as well as significantly increased ploidy (Figure 8F), indicative of increased endocycling. As predicted, these manipulations also led to significant increase in the tissue size of Zone 4 (Figure 8G.)

We tested whether increased ploidy led to altered peritrophic membrane synthesis by staining with a panel of molecular markers. Confocal projections of HPA lectin stained tissues revealed large areas of glycosylated material emanating from Zone 4, forming thickened cords that were not observed in controls (Figure 8B). To quantify this phenotype, we measured the cross-sectional area of HPA lectin-stained material adjacent to Zone 4 and found a significant

increase in *UAS:CycE* and *UAS:Myc* flies (Figure 8C and 8H). We then stained these tissues for calcofluor, which labels chitin, a major component of the layer of peritrophic membrane synthesized by Zone 4. We observed a significant increase in calcofluor-positive signal adjacent to Zone 4 in *UAS:CycE* and *UAS:Myc* flies, indicative of increased chitin synthesis (Figure 8D and 8I). Lastly, we stained these tissues with wheat germ agglutinin (WGA), an additional marker for glycosylated targets, and which has been used as a peritrophic membrane marker[55], and observed a significant increase in WGA staining adjacent to Zone 4 as well (Figure 8E and 8J). Together, these results suggest that increasing endocycling in Zone 4 leads to increased synthesis of peritrophic membrane in the proventriculus.

These experiments with *UAS-CycE* and *UAS-Myc* also allowed us to perform an independent test of whether endocycling was functionally causal for the loss of cells from Zone 4 during aging. If cell loss was driven by the process of tissue growth via endocycling, then experimentally increasing endocycling via *UAS-Myc* or *UAS-CycE* should lead to enhanced cell loss. We counted the number of GFP+ cells in these genotypes one day after shifting to 29ºC, and after 12 days (Supplementary Figure 9). The number of cells in each genotype decreased after 12 days by between 21% - 31%, but the percent decrease between genotypes were not significantly different (Supplementary Figure 9), despite the fact that ploidy, nuclear size, and tissue size is significantly increased in these genotypes compared to controls (Figure 8). This suggests that the loss of Zone 4 cells during aging is not driven by endocycling itself, and that a distinct mechanism must govern the loss of cells.

Blocking endocycling reduces peritrophic membrane synthesis. To inhibit endocycling, we used RNAi to knock down several candidate genes implicated in the regulation of the endocycle in *Drosophila*: *fizzy-related (fzr), E2F1, myc, CycE,* and the insulin receptor (*InR*)[12,56–64]. Of these candidates, *InR-RNAi* was by far the most potent reagent to block endocycling and reduce ploidy in Zone 4 (Supplementary Figure 10 and Figure 9). *fzr-RNAi* did not reduce ploidy (Supplementary Figure 10A), *E2F1-RNAi* caused a statistically significant yet relatively modest reduction in ploidy (Supplementary Figure 10B), and *myc-RNAi* led to dramatic disruptions to Zone 4 structure beyond simply blocking endocycling (Supplementary Figure 10C). While *cycE-RNAi* did reduce ploidy and tissue size (Supplementary Figure 10D,F,G), this effect was muted compared to *InR-RNAi* and caused large aggregations of peritrophic membrane material that complicated further analysis (Supplementary Figure 10D,E). Thus, we focused our analysis of inhibited endocycling to *InR-RNAi*, and we note the caveat that Insulin signaling has additional effects of cellular metabolism in addition to simply regulating the cell cycle.

Using two independent RNAi constructs, we observed a near total loss of EdU staining in *71F06-Gal4^{ts} > InR-RNAi* animals (Figure 9A,B) and a concordant failure to increase ploidy during aging (Figure 9C). In control flies (*71F06-Gal4^{ts} > w^{1118}* or *mCherry-RNAi*), Zone 4 nuclei steadily increase in ploidy between 6 days and 21 days at 29ºC, where in *71F06-Gal4^{ts} > InR-RNAi* flies, ploidy did not increase (Figure 9C). The overall size of Zone 4, visualized with cytoplasmic *UAS:2XEGFP,* was dramatically reduced by *InR-RNAi* (Figure 9D,H). These experiments also demonstrate that the link between systemic nutrition and endocycling in Zone

4 (e.g. Figure 1F-G) is at least partially regulated cell autonomously via insulin signaling directly interpreted by these cells.

We visualized the peritrophic membrane in *71F06-Gal4^{ts} > InR-RNAi* flies using the same three molecular markers as above. Consistent with the reduced nuclear volume and tissue size, the quantity of peritrophic membrane emanating from Zone 4 in *InR-RNAi* animals was significantly reduced, as revealed by staining for HPA lectin, calcofluor, and WGA (Figure 9E-G and 9I-K). These alterations in peritrophic membrane morphology are consistent with the hypothesis that increased genomic copies allow for increased synthesis of peritrophic membrane components.

The peritrophic membrane is continuously synthesized in the proventriculus, then migrates posteriorly to line the midgut, where it serves as a protective barrier for the absorptive surface of enterocytes[65,66]. To assess the ultimate functional consequences of reduced endocycling in Zone 4 cells, we performed a number of assays to characterize the structure and function of the peritrophic membrane in the midguts of *71F06-Gal4^{ts} > InR-RNAi* flies. When viewed using transmission electron microscopy (TEM), the peritrophic membrane can be seen to contain four distinct layers[16]. Zone 4 is thought to synthesize the contents the second layer, L2, which is chitin-rich and appears as a thick, electron-dense layer abutting the lumen [16] (Supplementary Figure 11A). We analyzed the peritrophic membrane of *InR-RNAi* flies using TEM (14 days at 29ºC), and did not observe any gross morphological defects or alterations to the four-layered structure (Supplementary Figure 11A), indicating that L2-containing peritrophic membrane is still produced in flies with reduced endocycling in Zone 4.

We then performed two independent assays for intestinal barrier integrity on *71F06-Gal4^{ts} > InR-RNAi* flies. First, we subjected *71F06-Gal4^{ts} > InR-RNAi* flies to the “smurf assay”, in which flies are fed a blue dye which leaks from the gut into the rest of the body in flies with a compromised gut barrier[67,68]. In flies which had been aged for 24 days at 29ºC, we did not observe any gut leakage either in controls or *71F06-Gal4^{ts} > InR-RNAi* flies (Supplementary Figure 11B), indicating that these guts retained a baseline of functional integrity. Similarly, when we fed flies with fluorescently-labeled beads (diameter 0.056 µm) to test for leakage[55,66], we did not detect a statistically significant increase in the proportion of *71F06-Gal4^{ts} > InR-RNAi* flies with leaky peritrophic membranes compared to controls (Supplementary Figure 11C). These two assays suggest that flies with inhibited endocycling in the proventriculus are still capable of producing sufficient peritrophic membrane to function under standard laboratory conditions.

The peritrophic membrane is a critical barrier to pathogens[66,69,70], so we hypothesized that reduced endocycling in Zone 4 cells may ultimately lead to functional defects in pathogen resistance. Under standard conditions at 29ºC, the lifespan *71F06-Gal4 > InR-RNAi* flies was indistinguishable from control flies (Figure 9L), consistent with the above observations that peritrophic membrane is not grossly malformed or dysfunctional. However, when these flies were challenged with the pathogenic bacteria *Pseudomonas aeruginosa* (*PA14*), *InR-RNAi* flies were significantly more susceptible to infection than controls (Figure 9M), indicating that the peritrophic membrane has compromised function. These results suggest that while continual

endocycling of Zone 4 cells is not strictly required for peritrophic membrane synthesis, it instead provides robustness in the face of environmental challenges such as pathogenic bacteria.

Altogether, these experiments demonstrate that endocycling leads to increased ploidy, tissue size, and synthetic capacity in Zone 4, ultimately increases the production of peritrophic membrane components. We propose that endocycling is a compensatory mechanism to ensure that continued production of sufficient quantities of peritrophic membrane components as cells are lost to aging or tissue damage.

Discussion. We find no evidence of stem cells in the *Drosophila* proventriculus, in contrast to a previous report [15]. Our experiments demonstrate that the EdU+ cells in Zone 4 do not undergo mitosis, do not produce clonal lineages, do not cycle in response to nearby tissue damage, and instead increase in ploidy throughout adulthood. These results suggest that the primary lines of evidence in support of the stem cell hypothesis were most likely the result of spontaneous, background MARCM activity as well as leaky expression of the Gal4 line used for lineage tracing[15].

We find that the cells in Zone 4 endocycle continuously throughout the fly's life, even in the absence of exogenous damage, and that a subset of these cells are shed into the gut lumen as the fly ages. We also demonstrate that, causally, Zone 4 cells endocycle in response to cell loss from the tissue, indicating that the cells can detect nearby cell loss. Functionally, we find that blocking endocycling in Zone 4 causes decreases peritrophic membrane synthesis. Our experiments reveal that flies are remarkably robust in the face of this reduced peritrophic membrane levels, and do not show obvious ultrastructural defects or gut leakage. However, flies with endocycle-deficient proventriculi are less resistant to potent bacterial pathogen infection. Thus, we propose that continual endocycling in Zone 4 ensures sufficient levels of peritrophic membrane synthesis throughout the fly's life to address the diversity of environmental challenges that flies may experience in the wild.

Endoreplication and polyploidy are both widespread in *Drosophila* and across animals and plants, both under healthy, homeostatic conditions and in response to cell or tissue damage[31,50,51,71,72]. In the *Drosophila* larva, many tissues cease mitotic proliferation during embryogenesis, and subsequently grow via developmentally programmed endocycling[31,73]. In adult flies, many cell types become polyploid via endoreplication under wildtype conditions, including the nurse cells and follicle cells of the ovary, the enterocytes of the midgut, and rectal papillae cells[71], while other cell types endocycle in response to tissue or cellular damage, including the epidermis in response to wounding[13,71], the hindgut in response to tissue injury[11,12], and the adult brain in response to oxidative and DNA damage[74]. Mammals also display widespread examples of both developmentally programmed endocycling as well as damage-responsive endocycling, including for example in the mammalian liver which displays high levels of endoreplication in response to damage and injury[31,50,51,71,72].

The pattern of endocycling that we observe in the proventriculus appears to differ in certain respects from several other well-characterized examples of endoreplication in *Drosophila* and

other tissues. Unlike ectodermal gut regions including the hindgut[11,12] or the esophagus (Figure 5E), endoreplication in the proventriculus appears to occur throughout the fly's life, even in the absence of exogenous tissue injury. Whereas many other highly metabolically active cells become highly polyploid via endoreplication, including the nurse cells or the follicle cells of the ovary, in those cell types endoreplication appears to proceed for a specific number of cycles and then cease[75], rather than continual endoreplication over the fly's lifespan. What we observe in the proventriculus is a continuous increase in ploidy throughout the adult stage, as part of a homeostatic system that accounts for the steady loss of neighboring cells and responds to the nutritional input of the fly. A similar progressive increase in cell ploidy is seen in the adult brain, where several neuronal and glial cell types that are diploid at eclosion become polyploid during aging in response to DNA damage or oxidative stress [74].

Interestingly, we observe consistent endocycling in young flies including during the first two weeks of the adult stages (Figure 6A-C), a period in which we detect very modest age-related cell loss (Figure 6D). This indicates that endocycling is a consistent feature of this tissue throughout the fly's life, and not solely a response to cell loss. A possible explanation for this consistent endocycling of cells at the posterior edge of Zone 4 is that the production of peritrophic membrane components is intrinsically damaging to these cells, given the very high synthetic and secretory demands of this process. In the midgut, the inherent cellular functions of the enterocytes are thought to cause high levels of cellular stress and thereby require consistent replacement via stem cells, even in the absence of acute tissue damage. Given the absence of stem cells in Zone 4, continual endocycling may serve a similar function in this tissue, to maintain a functional baseline of synthetic and secretory activity as the tissue accrues damage due to the cellular stress of peritrophic membrane synthesis. There are similar examples of polyploidization in response to cell loss during aging or disease, including in the mammalian cornea, where cell loss due to disease can be compensated for by polyploidization of remaining cells[14].

We propose that there are two distinct stages of endocycling in the *Drosophila* proventriculus: first, during the first ~14d of a fly's life, regular endocycling at the posterior edge of Zone 4 steadily increases the size of the tissue. Then, as the fly ages and cells are increasingly lost from Zone 4, the surviving cells increase endocycling in order to compensate for the loss of these cells. Interestingly, because the ploidy of these cells steadily increases with age, we propose that it may be possible to estimate the age of a fly based on the distribution of ploidies observed in Zone 4.

Altogether, we propose that this system may provide insights into how the endocycle can be regulated over long timescales, as well as into the mechanisms that link age-related cell loss to endoreplication.

Methods

Experimental animals. Genotypes and sources for *Drosophila melanogaster* lines used in this study are provided in Supplementary Table 1. Flies were maintained at 18ºC, 25ºC, 29ºC, as

indicated in the text, on standard laboratory cornmeal food, except for EdU treatments, yeast supplementation experiments, or drug treatments, which were maintained on Formula 4-24 Instant Blue Food ("Instant Blue Food", Carolina Biological Supply) as described below. All experiments were performed on female flies. No ethical approval was required for studies on *Drosophila melanogaster*.

Except where noted in the text, all experiments were initiated on flies within 1 week of eclosion, and all flies were age-matched within an experiment. For temperature shift experiments with *tubGal80*^{ts}, flies were reared throughout development at 18ºC and were shifted to 29ºC 1-4 days after eclosing.

EdU feeding and EdU+ cell counting. EdU (Thermo Fisher) was diluted to 0.2mM in water, then used to hydrate an equal volume of Carolina Instant Blue Food, supplemented with yeast powder as indicated in the text. Adult flies were transferred to EdU-containing food, and flipped to fresh EdU-containing food every two days, for any experiment lasting longer than two days. EdU signal was detected using Click-iT™ EdU Cell Proliferation Kit (Thermo Fisher). Except where noted in the text, 5% yeast was used in EdU experiments (100 mg dried yeast per 2 mL of food), and flies were < 2 weeks old. EdU+ cells were manually counted on a compound epifluorescent microscope, specifically focusing on those EdU+ cells located in Zone 4. Unless otherwise noted in the text, flies were fed EdU for two days prior to dissection.

Yeast variation experiments. To test the effect of supplemental dietary yeast on EdU incorporation, dried active yeast was added as a percentage by weight of Instant Blue Food.

Colchicine treatment. To enrich mitotic nuclei, flies were fed with 0.2 mg/mL colchicine (EMD Millipore) for 12 hours prior to dissection. Colchicine was diluted in water and used to dilute Instant Blue Food supplemented with 10% yeast.

Gut damage with X-rays, bleomycin, and *ECC15* infection. For X-ray damage, adult flies were irradiated with 0, 1000, or 2000 RADs in a TORREX 120D X-ray Inspection System (ScanRay Corporation). For gut damage with bleomycin, bleomycin (Sigma) was diluted to 25 ng/µL in water and used to rehydrate 2 mL of Instant Blue Food. Flies were fed bleomycin-contained food for two days at 29ºC to increase ingestion, and were flipped to fresh food each day, with water as a control. For *ECC15* treatment, 100mL of LB medium were inoculated with 20 µL of a *ECC15* glycerol stock and grown at 30ºC for 20-24 hours. *ECC15* cultures were then centrifuged for 30 minutes at 1810 x g and resuspended in 1.4 mL of a 5% sucrose. Flies were starved for two hours at 29ºC, and then flipped to a vial containing only a kimwipe soaked in 700 µL of the *ECC15* solution, where they fed for 24 hours at 29ºC to induce gut damage. After gut damage, flies were maintained on standard food at 25ºC for the indicated amount of time.

Immunohistochemistry and confocal imaging. Tissues were dissected in 1X phospho-buffered saline (PBS), fixed for 25-30 minutes in 4% paraformaldehyde in PBS, permeabilized in PBS with 0.3% Triton-X (PBST), and stained following standard antibody staining procedures using 5% normal goat serum as a blocking agent. Filamentous actin was stained using Alexa

555-coupled phalloidin (Molecular Probes), peritrophic membranes were stained with Alexa647-coupled HPA lectin (1:100, Thermo Fisher), calcofluor white stain (1:100, Sigma-Aldrich), Alexa647-coupled wheat germ agglutinin (1:400, Fisher Scientific) and nuclei were stained using DAPI. For HPA Lectin, we found that an incubation of at least two nights at 4ºC, and up to five nights, was necessary for reliable staining, whereas calcofluor and WGA were stained overnight for two nights, and that these peritrophic membrane stainings were improved by isolating the anterior midgut below the proventriculus from the rest of the midgut. Stained tissues were mounted in Vectashield (Vector Labs), except for Alexa647-labeled tissues which were mounted in Prolong Gold (Thermo Fisher Scientific). Rabbit anti-GFP AlexaFluor488 conjugate (Molecular Probes, 1:300) was used to visualize GFP expression, Wg expression was detected using mouse anti-Wg (Developmental Studies Hybridoma Bank 4D4, 1:100) and phospho-Histone 3 was detected using rabbit anti-PH3 (Cell Signaling Technologies 9701S, 1:500). Primary antibodies were detected with Alexa Fluor 488- or 555- coupled secondary antibodies (1:400). Confocal images were captured on a Zeiss LSM 780, LSM 980, or an Olympus IX83 confocal microscope, through the Microscopy Resources of the North Quad (MicRoN) facility at Harvard Medical School.

Single nucleus RNAseq (snRNAseq) atlas. To capture proventriculus transcriptional states in both well-fed flies and flies with reduced systemic insulin signaling, single nuclei suspensions were generated from proventriculus samples from both control flies (*esg-Gal4, tubGal80^{ts}, UAS:GFP /* +) and cachexic flies (*esg-Gal4, tubGal80^{ts}, UAS:GFP ; UAS-yki^{3SA}*), after 8 or 9 days at 29ºC. We verified via confocal analysis that *esg-Gal4* is not expressed in the proventriculus itself, which was also confirmed via snRNA sequencing. Proventriculus samples were manually dissected from adult female flies in cold Schneider's medium and immediately flash frozen on dry ice in eppendorf tubes until a total of approximately 600 samples were collected (~300 of each genotype). Proventriculi were manually severed from the crop and esophagus, and from the midgut just posterior to the proventriculus, anterior to where *esg-Gal4* is detected in midgut ISCs.

Single nuclei were isolated following the protocol described in[76], derived originally from[77], and stained with DAPI immediately before FACS sorting, performed at the Immunology Flow Cytometry Core at Harvard Medical School. Sorted nuclei were resuspended in 1X PBS supplemented with 0.5% BSA with RNAse inhibitor (Promega) at a concentration of ~2000 cells/µl.

snRNAseq was performed following the 10X Genomics Chromium protocol (Chromium Next GEM 551 Single Cell 3'_v3.1_Rev_D), and sequenced using a Illumina NovaSeq 6000 at the Harvard Medical School Biopolymers Facility. 10,525 nuclei from *esg^{ts}* flies and 11,801 nuclei from esg^{ts} > *yki* flies were sequenced (total = 22,332 nuclei) and reads were mapped to BDGP6.32.

Bioinformatic analysis was performed as follows, and the analysis pipeline is available here: https://github.com/MujeebQadiri/SingleNucleiProventriculusAnalysis/tree/main. Raw data were processed with Cell Ranger software (10x Genomics, v7.0.0) to generate a single cell matrix for

each sample. The count matrices were imported into Seurat (v4.3.0) and cells with less than 1300 or greater than 60,000 UMIs were filtered out, and low abundance genes with less than 10 counts were removed from further analysis. The two biological samples were bioinformatically pooled for PCA and clustering analysis to generate a single atlas including cells from both conditions. After a PCA reduction, the first 40 components were used for UMAP and clustering analysis, at a 0.2 resolution. We removed from further analysis one cluster that appeared to be an artefact, as it contained markers for multiple different unrelated cell-types as well as stress and heat shock proteins. Differentially expressed genes were calculated using the Wilcox Rank Sum Test across each cluster and were then further selected using a Log2FC > X cut-off and adjusted p value < 0.05. All downstream analysis was performed in R (v4.3).

To map snRNAseq clusters to proventriculus anatomy, we examined the expression pattern of Gal4 lines for top-ranking marker genes using confocal microscopy.

MARCM analysis. Flies of the genotype *hsFLP, FRT19A, tubGal80 ; tub-Gal4, UAS-GFP* were crossed to *FRT19A* flies (BL1709), and offspring were heat-shocked in a 37ºC water bath either during the L3 stage for during the adult stage. Two one hour heat-shocks were administered, separated by 2-3 hours at 25ºC. MARCM crosses were maintained at either 25ºC or 18ºC as indicated in the text.

Tissue damage protocol using *UAS-rpr.* We induced ectopic apoptosis by crossing Gal4 drivers to flies containing *UAS-rpr*; *tubGal80^{ts}* or, for non-damaged controls, to *w^{1118}* flies. These crosses were maintained at 18ºC until several days after eclosion. Adult flies were then transferred to EdU+ food and placed at 29ºC for 48 hours to induce apoptosis. For recovery experiments, flies then returned to recover at 18ºC for either 2 days or 5 days, on EdU+ food throughout. For continuous damage experiments, flies were maintained at 29ºC for either 2 or 5 days. Thus, all EdU+ incorporation events that occurred during the damage or during the recovery period could be visualized and quantified.

Creation of split-intein Gal4 line. To generate *GMR71F06::Gal4-C-int*, the 3,547 bp enhancer fragment from *GMR71F06* FlyLight line[79] was amplified using the following primers: caccTGCCCCGAGCAGCAAAAGAAGTCCG and TCTCCGAAATCTGCGCCAATTCCAG, and cloned into the pENTR-dTOPO vector (Thermo Fisher Scientific). This fragment was cloned into the pBP-Gal4$^{C\text{-}int}$ backbone[39] (Addgene 199202) via LR gateway cloning, and was inserted into the attP40 landing site using standard phiC31 transgenesis.

Time series of nuclear morphology and EdU incorporation. To quantify ploidy and nuclear morphology over the course of the fly's life, age matched flies of the genotype *GMR7106-Gal4 / UAS-Stinger ; MKRS /* + were collected on eclosion day, and maintained at 25ºC in standard fly vials on standard lab food (approximately 10-15 adult flies per vial), either with or without dried active yeast sprinkled on the food's surface. In a pilot experiment, we observed that *UAS-Stinger* is tightly nuclear-localized in this tissue, whereas other common nuclear-localized fluorophores transgenes (*UAS:GFP^{NLS}* [BL4776], *UAS-unc84-GFP* [lab stock] and *UAS:RedStinger* [BL8545]) were not. Flies were flipped onto fresh food every two or three days.

On each day of sampling (3d, 7d, 14, 21d, 28d, and 35d), approximately 6-8 cardia were dissected and stained overnight with Alexa 488-coupled anti-GFP, DAPI, and phalloidin as described above. At each time-point, confocal z-stacks were collected through the entirety of Zone 4 (n=5-6 proventriculus per time point) and analyzed as described below. We also collected samples for eclosion day and for 1d later, but found that the Gal4 expression pattern extended beyond Zone 4 at these time points, so they were excluded from further analysis.

For *OregonR* aging experiments with EdU, batches of flies were collected on the day that they eclosed and then aged at 25ºC on standard food with yeast powder until the indicated ages. Flies were transferred to EdU+ food two days prior to EdU+ food. Anterior-posterior position was calculated from confocal stacks by measuring the shortest distance between the center of each EdU+ and the vertical center of the posterior-most row of cells in Zone 4, hence EdU+ cells located in the posterior-most row were measured as zero.

Image quantification. Ploidy was analyzed from DAPI-stained confocal z-stacks, following a protocol modified from[80] and described below, using FIJI software[81]. A subset of the confocal z-stack containing only a single layer of nuclei from the surface of Zone 4 was generated using the "sum intensity" projection method, and region-of-interests were manually drawn for each visible Zone 4 nucleus using *71F06-Gal4 > GFP* signal to ensure that all nuclei measured were in Zone 4. Summed DAPI intensity was calculated using the "integrated density" function. To normalize these values, we used diploid nuclei from Zone 3 as an internal control within each sample. We determined Zone 3 cells to be diploid by direct comparison to diploid ISCs captured under identical imaging parameters. Thus, a diploid standard was calculated for each sample from an averaged value of of approximately 15-25 diploid cells within each confocal stack.

Additional nuclear quantification, including cell volume and cell counts were performed with arivis Vision4D software (Zeiss, v4.1.2). GFP+ nuclei were segmented using the Cellpose-based Segmenter, and segmentation was then manually corrected for each sample by splitting or removing nuclei which were erroneously fused and removing artefacts that did not correspond to nuclei. Nuclear volume was extracted for all objects >10μm^3. For cell count, those nuclei missed by Cellposed-based segmentation were manually counted using the "add marker" function while viewing the tissue in 3D. To quantify cell loss during aging, cells that had been shed into the lumen were manually counted in FIJI[81].

As a measure of tissue size for Zone 4, we measured the area of Zone 4 at the widest point of the proventriculus. Each sample value represents the averaged area of two independent measurements of cross-sections of Zone 4, on either sides of the esophagus. For area measurements of peritrophic membrane features stained with HPA lectin, WGA, or calcofluor, we made a maximum intensity projection of 3-4 confocal z-slices at the equator of the proventriculus, and measured the area of stained material, averaging two measurements taken for each sample on either side of the esophagus.

Peritrophic membrane electron microscopy and leakiness assays. "Smurf" assays were performed as previously described [67], as follows. Flies transferred to standard lab food

containing 2.5% FD&C Blue #1 dye (Spectrum) by weight, and were examined for gut leakiness after 24 and 48 hours. Any flies where blue food was restricted to the proboscis, crop, and gut was scored as wildtype.

Fluorescent bead leakiness analysis were performed similar to previous reports [55,66]. Flies were starved in empty vials for 2 hours at 29ºC, then transferred to vials containing half of a standard kimwipe saturated with a 1:50 dilution of Fluoresbrite YG microbeads (diameter 0.056 µm; Polysciences) in 5% sucrose. Flies were dissected between 30-60 minutes after feeding, and whole guts were fixed and stained with DAPI and phalloidin and/or HPA lectin as described above. Guts were scored under 40X magnification as either intact or containing leaky regions where fluorescent beads were visible outside of the peritrophic membrane.

Electron microscopy was performed in the Harvard Electron Micrscopy Facility. Tissues were prepared as described [69], and longitudinally sectioned anterior midguts were imaged using a Tecnai G2 BioTwin microscope.

Lifespan and *Pseudomonas* survival experiments. Lifespan experiments were conducted at 29ºC, with 15 mated females per vial on standard fly food supplemented with dried yeast powder, and flipped every 1-2 days. Flies of the genotype *w ; tubGal80^{ts} , UAS:GFP ; 71F06-Gal4* were crossed to control or UAS:RNAi lines, and the offspring were reared at 18ºC until eclosion. Adults were collected and mated over a 4 day period at 18ºC, then shifted to 29ºC three days later to begin life-span measurements. The number of dead flies was recorded every day.

Infection with *Pseudomonas aeruginosa (PA14)* followed a protocol similar to[69]. 5mL of LB medium was seeded from a glycerol stock of *PA14* and grown overnight in a shaking 37ºC incubator. The following morning, 1 mL of this culture was diluted in 50 mL of fresh LB and grown for an additional 6 hours, shaking at 37ºC. This culture was then diluted 1:3 in 5% sucrose solution. Fly vials containing half of a standard kimwipe, compressed into the bottom of the vial, were loaded with 1.5 mL of this bacterial suspension. In order to promote feeding on the bacteria, flies were starved for two hours in empty vials immediately prior to bacterial treatment.

These experiments were performed at 29ºC on flies that had been maintained at 29ºC for 15 days prior to *PA14* infection. After a 24 hour infection, flies were flipped to fresh vials containing kimwipes saturated with 5% sucrose solution, and flipped to fresh 5% sucrose solution daily after that. The number of dead flies was recorded approximately every 24 hours. Four vials of 8-10 flies each were used per genotype, and the entire experiment was performed in biological duplicate, with similar results in both experiments.

Graphing and statistical analysis. All graphs were created and statistical tests performed using Prism (GraphPad, v10).

Data Availability

The snRNA-seq data generated in this study have been deposited in the NCBI Gene Expression Omnibus (GEO) database under accession code GSE301009 [https://www.ncbi.nlm.nih.gov/geo/query/acc.cgi?acc=GSE301009]. The snRNA-seq Atlas is available for data mining at https://www.flyrnai.org/scRNA/. The raw data used to generate all figures are provided as a Source Data file.

Code Availability

Scripts used to analyze snRNAseq data are provided here: https://github.com/MujeebQadiri/SingleNucleiProventriculusAnalysis/tree/main.

References

1. Buchon, N. & Osman, D. All for one and one for all: Regionalization of the *Drosophila* intestine. *Insect Biochem Molec* **67**, 2–8 (2015).

2. Buchon, N. *et al.* Morphological and Molecular Characterization of Adult Midgut Compartmentalization in *Drosophila*. *Cell Reports* **3**, 1725–1738 (2013).

3. O'Brien, L. E. Regional Specificity in the *Drosophila* Midgut: Setting Boundaries with Stem Cells. *Cell Stem Cell* **13**, 375–376 (2013).

4. Micchelli, C. A. & Perrimon, N. Evidence that stem cells reside in the adult *Drosophila* midgut epithelium. *Nature* **439**, 475–479 (2005).

5. Ohlstein, B. & Spradling, A. The adult *Drosophila* posterior midgut is maintained by pluripotent stem cells. *Nature* **439**, 470–474 (2006).

6. Lucchetta, E. M. & Ohlstein, B. The *Drosophil*a midgut: a model for stem cell driven tissue regeneration. *Wiley Interdiscip. Rev.: Dev. Biol.* **1**, 781–788 (2012).

7. Jiang, H., Tian, A. & Jiang, J. Intestinal stem cell response to injury: lessons from *Drosophila*. *Cell. Mol. Life Sci.* **73**, 3337–3349 (2016).

8. Cheng, H. & Leblond, C. P. Origin, differentiation and renewal of the four main epithelial cell types in the mouse small intestine V. Unitarian theory of the origin of the four epithelial cell types. *Am. J. Anat.* **141**, 537–561 (1974).

9. Barker, N. *et al.* Identification of stem cells in small intestine and colon by marker gene Lgr5. *Nature* **449**, 1003–1007 (2007).

10. Zwick, R. K., Ohlstein, B. & Klein, O. D. Intestinal renewal across the animal kingdom: comparing stem cell activity in mouse and *Drosophila*. *Am. J. Physiol.-Gastrointest. Liver Physiol.* **316**, G313–G322 (2019).

11. Fox, D. T. & Spradling, A. C. The *Drosophila* Hindgut Lacks Constitutively Active Adult Stem Cells but Proliferates in Response to Tissue Damage. *Cell Stem Cell* **5**, 290–297 (2009).

12. Cohen, E., Allen, S. R., Sawyer, J. K. & Fox, D. T. Fizzy-Related dictates A cell cycle switch during organ repair and tissue growth responses in the *Drosophila* hindgut. *eLife* **7**, e38327 (2018).

13. Losick, V. P., Fox, D. T. & Spradling, A. C. Polyploidization and Cell Fusion Contribute to Wound Healing in the Adult *Drosophila* Epithelium. *Curr. Biol.* **23**, 2224–2232 (2013).

14. Losick, V. P., Jun, A. S. & Spradling, A. C. Wound-Induced Polyploidization: Regulation by Hippo and JNK Signaling and Conservation in Mammals. *PLoS ONE* **11**, e0151251 (2016).

15. Singh, S. R., Zeng, X., Zheng, Z. & Hou, S. X. The adult *Drosophila* gastric and stomach organs are maintained by a multipotent stem cell pool at the foregut/midgut junction in the cardia (proventriculus). *Cell Cycle* **10**, 1109–1120 (2011).

16. King, D. G. Cellular organization and peritrophic membrane formation in the cardia (Proventriculus) of *Drosophila* melanogaster. *J. Morphol.* **196**, 253–282 (1988).

17. Wigglesworth, V. B. The Formation of the Peritrophic Membrane in Insects, with Special Reference to the Larvae of Mosquitoes. *J. Cell Sci.* **s2-73**, 593–616 (1930).

18. Rizki, M. T. M. The secretory activity of the proventriculus of *Drosophila* melanogaster. *J. Exp. Zoöl.* **131**, 203–221 (1956).

19. Pankratz, M. J. & Hoch, M. Control of epithelial morphogenesis by cell signaling and integrin molecules in the *Drosophila* foregut. *Development* **121**, 1885–1898 (1995).

20. Fuß, B. & Hoch, M. *Drosophila* endoderm development requires a novel homeobox gene which is a target of Wingless and Dpp signalling. *Mech. Dev.* **79**, 83–97 (1998).

21. Fuss, B., Josten, F., Feix, M. & Hoch, M. Cell movements controlled by the Notch signalling cascade during foregut development in *Drosophila*. *Development* **131**, 1587–1595 (2004).

22. Waterhouse, D. The Rate of Production of the Peritrophic Membrane in Some Insects. *Aust. J. Biol. Sci.* **7**, 59–72 (1954).

23. Becker, B. Determination of the formation rate of peritrophic membranes in some Diptera. *J. Insect Physiol.* **24**, 529–533 (1978).

24. Tzou, P. *et al.* Tissue-Specific Inducible Expression of Antimicrobial Peptide Genes in *Drosophila* Surface Epithelia. *Immunity* **13**, 737–748 (2000).

25. Zhu, H., Ludington, W. B. & Spradling, A. C. Cellular and molecular organization of the *Drosophila* foregut. *Proc. Natl. Acad. Sci.* **121**, e2318760121 (2024).

26. Dodge, R. *et al.* A symbiotic physical niche in *Drosophila* melanogaster regulates stable association of a multi-species gut microbiota. *Nat. Commun.* **14**, 1557 (2023).

27. Bertran-Mas, J., Giorgio, E. D., Martín, N. & Llimargas, M. Distinct cellular and molecular mechanisms contribute to the specificity of the two *Drosophila melanogaster* chitin synthases in chitin deposition. *PLOS Genet.* **21**, e1011847 (2025).

28. Pandey, A. *et al.* Gut barrier defects, intestinal immune hyperactivation and enhanced lipid catabolism drive lethality in NGLY1-deficient *Drosophila*. *Nat. Commun.* **14**, 5667 (2023).

29. Zhang, L., Turner, B., Ribbeck, K. & Hagen, K. G. T. Loss of the mucosal barrier alters the progenitor cell niche via Janus kinase/signal transducer and activator of transcription (JAK/STAT) signaling. *J. Biol. Chem.* **292**, 21231–21242 (2017).

30. Britton, J. S. & Edgar, B. A. Environmental control of the cell cycle in *Drosophila*: nutrition activates mitotic and endoreplicative cells by distinct mechanisms. *Development* **125**, 2149–2158 (1998).

31. Edgar, B. A. & Orr-Weaver, T. L. Endoreplication Cell Cycles More for Less. *Cell* **105**, 297–306 (2001).

32. Kwon, Y. *et al.* Systemic Organ Wasting Induced by Localized Expression of the Secreted Insulin/IGF Antagonist ImpL2. *Dev. Cell* **33**, 36–46 (2015).

33. Ding, G. *et al.* Coordination of tumor growth and host wasting by tumor-derived Upd3. *Cell Rep.* **36**, 109553 (2021).

34. Liu, Y., Saavedra, P. & Perrimon, N. Cancer cachexia: lessons from *Drosophila*. *Dis. Model. Mech.* **15**, dmm049298 (2022).

35. Lim, S. Y. *et al.* Identification and characterization of GAL4 drivers that mark distinct cell types and regions in the *Drosophila* adult gut. *J. Neurogenet.* **35**, 33–44 (2021).

36. Ghosh, S. *et al.* A local insulin reservoir in *Drosophila* alpha cell homologs ensures developmental progression under nutrient shortage. *Curr. Biol.* **32**, 1788-1797.e5 (2022).

37. Kim, S. K. & Rulifson, E. J. Conserved mechanisms of glucose sensing and regulation by *Drosophila* corpora cardiaca cells. *Nature* **431**, 316–320 (2004).

38. Lee, G. & Park, J. H. Hemolymph Sugar Homeostasis and Starvation-Induced Hyperactivity Affected by Genetic Manipulations of the Adipokinetic Hormone-Encoding Gene in *Drosophila* melanogaster. *Genetics* **167**, 311–323 (2004).

39. Ewen-Campen, B. *et al.* split-intein Gal4 provides intersectional genetic labeling that is repressible by Gal80. *Proc. Natl. Acad. Sci. United States Am.* **120**, e2304730120 (2023).

40. Hung, R.-J. *et al.* A cell atlas of the adult *Drosophila* midgut. *Proc National Acad Sci* **117**, 1514–1523 (2020).

41. Ren, F. *et al.* Hippo signaling regulates Drosophila intestine stem cell proliferation through multiple pathways. *Proc National Acad Sci* **107**, 21064–21069 (2010).

42. Karpowicz, P., Perez, J. & Perrimon, N. The Hippo tumor suppressor pathway regulates intestinal stem cell regeneration. *Development (Cambridge, England)* **137**, 4135–4145 (2010).

43. Shaw, R. L. *et al.* The Hippo pathway regulates intestinal stem cell proliferation during *Drosophila* adult midgut regeneration. *Development* **137**, 4147–4158 (2010).

44. Jiang, H., Grenley, M. O., Bravo, M.-J., Blumhagen, R. Z. & Edgar, B. A. EGFR/Ras/MAPK Signaling Mediates Adult Midgut Epithelial Homeostasis and Regeneration in *Drosophila*. *Cell Stem Cell* **8**, 84–95 (2011).

45. Xu, C., Luo, J., He, L., Montell, C. & Perrimon, N. Oxidative stress induces stem cell proliferation via TRPA1/RyR-mediated Ca2+ signaling in the *Drosophila* midgut. *eLife* **6**, e22441 (2017).

46. Leung, N. Y. *et al.* Gut tumors in flies alter the taste valence of an anti-tumorigenic bitter compound. *Curr. Biol.* **34**, 2623-2632.e5 (2024).

47. McLeod, C. J., Wang, L., Wong, C. & Jones, D. L. Stem cell dynamics in response to nutrient availability. *Current biology : CB* **20**, 2100–2105 (2010).

48. Lucchetta, E. M. & Ohlstein, B. Amitosis of Polyploid Cells Regenerates Functional Stem Cells in the *Drosophila* Intestine. *Stem Cell* **20**, 1–19 (2017).

49. Evans, C. J. *et al.* G-TRACE: rapid Gal4-based cell lineage analysis in *Drosophila*. *Nat Methods* **6**, 603–5 (2009).

50. Morris, J. P., Baslan, T., Soltis, D. E., Soltis, P. S. & Fox, D. T. Integrating the Study of Polyploidy Across Organisms, Tissues, and Disease. *Annu. Rev. Genet.* (2024) doi:10.1146/annurev-genet-111523-102124.

51. Øvrebø, J. I. & Edgar, B. A. Polyploidy in tissue homeostasis and regeneration. *Development* **145**, dev156034 (2018).

52. Molano-Fernández, M., Hickson, I. D. & Herranz, H. Cyclin E overexpression in the *Drosophila* accessory gland induces tissue dysplasia. *Front. Cell Dev. Biol.* **10**, 992253 (2023).

53. Demontis, F. & Perrimon, N. Integration of Insulin receptor/Foxo signaling and dMyc activity during muscle growth regulates body size in *Drosophila*. *Development (Cambridge, England)* **136**, 983–993 (2009).

54. Pierce, S. B. *et al.* dMyc is required for larval growth and endoreplication in *Drosophila*. *Development* **131**, 2317–2327 (2004).

55. Katheder, N. S. *et al.* Nicotinic acetylcholine receptor signaling maintains epithelial barrier integrity. *eLife* **12**, e86381 (2023).

56. Sigrist, S. J. & Lehner, C. F. *Drosophila* fizzy-related Down-Regulates Mitotic Cyclins and Is Required for Cell Proliferation Arrest and Entry into Endocycles. *Cell* **90**, 671–681 (1997).

57. Lehner, C. F. & O'Farrell, P. H. Expression and function of *Drosophila* cyclin a during embryonic cell cycle progression. *Cell* **56**, 957–968 (1989).

58. Schaeffer, V., Althauser, C., Shcherbata, H. R., Deng, W.-M. & Ruohola-Baker, H. Notch-Dependent Fizzy-Related/Hec1/Cdh1 Expression Is Required for the Mitotic-to-Endocycle Transition in *Drosophila* Follicle Cells. *Curr. Biol.* **14**, 630–636 (2004).

59. Losick, V. P. & Duhaime, L. G. The endocycle restores tissue tension in the *Drosophila* abdomen post wound repair. *Cell Rep.* **37**, 109827 (2021).

60. Zielke, N. *et al.* Control of *Drosophila* endocycles by E2F and CRL4CDT2. *Nature* **480**, 123–127 (2011).

61. Bellosta, P. & Gallant, P. Myc Function in *Drosophila*. *Genes Cancer* **1**, 542–546 (2010).

62. Grendler, J., Lowgren, S., Mills, M. & Losick, V. P. Wound-induced polyploidization is driven by Myc and supports tissue repair in the presence of DNA damage. *Development* **146**, dev173005 (2019).

63. Scalia, P., Williams, S. J., Fujita-Yamaguchi, Y. & Giordano, A. Cell cycle control by the insulin-like growth factor signal: at the crossroad between cell growth and mitotic regulation. *Cell Cycle* **22**, 1–37 (2023).

64. Jouandin, P., Ghiglione, C. & Noselli, S. Starvation induces FoxO-dependent mitotic-to-endocycle switch pausing during *Drosophila* oogenesis. *Development* **141**, 3013–3021 (2014).

65. Lehane, M. J. Peritrophic Matrix Structure AND Function. *Annu. Rev. Èntomol.* **42**, 525–550 (1997).

66. Kuraishi, T., Binggeli, O., Opota, O., Buchon, N. & Lemaitre, B. Genetic evidence for a protective role of the peritrophic matrix against intestinal bacterial infection in *Drosophila* melanogaster. *Proc. Natl. Acad. Sci.* **108**, 15966–15971 (2011).

67. Rera, M. *et al.* Modulation of Longevity and Tissue Homeostasis by the *Drosophila* PGC-1 Homolog. *Cell Metab.* **14**, 623–634 (2011).

68. Rera, M., Clark, R. I. & Walker, D. W. Intestinal barrier dysfunction links metabolic and inflammatory markers of aging to death in *Drosophila*. *Proc. Natl. Acad. Sci.* **109**, 21528–21533 (2012).

69. Kim, K., Hung, R.-J. & Perrimon, N. miR-263a Regulates ENaC to Maintain Osmotic and Intestinal Stem Cell Homeostasis in *Drosophila*. *Dev. Cell* **40**, 23–36 (2017).

70. Kim, K. *et al. Drosophila* as a model for studying cystic fibrosis pathophysiology of the gastrointestinal system. *Proc. Natl. Acad. Sci.* **117**, 10357–10367 (2020).

71. Fox, D. T. & Duronio, R. J. Endoreplication and polyploidy: insights into development and disease. *Development* **140**, 3–12 (2012).

72. Bailey, E. C., Kobielski, S., Park, J. & Losick, V. P. Polyploidy in Tissue Repair and Regeneration. *Cold Spring Harb. Perspect. Biol.* **13**, a040881 (2021).

73. Smith, A. V. & Orr-Weaver, T. L. The regulation of the cell cycle during *Drosophila* embryogenesis: the transition to polyteny. *Development* **112**, 997–1008 (1991).

74. Nandakumar, S., Grushko, O. & Buttitta, L. A. Polyploidy in the adult *Drosophila* brain. *eLife* **9**, e54385 (2020).

75. Zielke, N., Edgar, B. A. & DePamphilis, M. L. Endoreplication. *Cold Spring Harb. Perspect. Biol.* **5**, a012948 (2013).

76. Liu, Y. *et al.* Tumor Cytokine-Induced Hepatic Gluconeogenesis Contributes to Cancer Cachexia: Insights from Full Body Single Nuclei Sequencing. *bioRxiv* 2023.05.15.540823 (2023) doi:10.1101/2023.05.15.540823.

77. Li, H. *et al.* Fly Cell Atlas: A single-nucleus transcriptomic atlas of the adult fruit fly. *Science* **375**, eabk2432 (2022).

78. Saavedra, P. *et al.* REPTOR and CREBRF encode key regulators of muscle energy metabolism. *Nat. Commun.* **14**, 4943 (2023).

79. Jenett, A. *et al.* A GAL4-Driver Line Resource for *Drosophila* Neurobiology. *Cell Reports* **2**, 991–1001 (2012).

80. Clay, D. E., Stormo, B. M. & Fox, D. T. Measuring Cellular Ploidy In Situ by Light Microscopy. *Methods Mol. Biol. (Clifton, NJ)* **2545**, 401–412 (2023).

81. Schindelin, J. *et al.* Fiji: an open-source platform for biological-image analysis. *Nat. Methods* **9**, 676–682 (2012).

Acknowledgements

We thank Mujeeb Qadiri, Austin Veal, and Aram Comjean for assistance with snRNAseq data analysis and sharing, and Rich Binari for assistance with fly work. We thank Hannah Dayton and Liz Lane for reagents and advice with *Pseudomonas* experiments. We thank our three anonymous Reviewers for proposing several experiments and ideas which improved our study. This work was supported by the National Institute of Health R24 OD031952 awarded to NP. NP is an investigator of the Howard Hughes Medical Institute. This article is subject to HHMI's Open Access to Publications policy. HHMI lab heads have previously granted a nonexclusive CC BY 4.0 license to the public and a sublicensable license to HHMI in their research articles. Pursuant to those licenses, the author-accepted manuscript of this article can be made freely available under a CC BY 4.0 license immediately upon publication.

Author Contributions

B.E.C. conceived of the study, designed and performed all experiments, analyzed data, and wrote the manuscript with supervision from N.P. and input from all authors. S.G.T. and Y.L. assisted with the creation of the snRNAseq atlas, and W.C. and Y.H. performed bioinformatic analysis of the snRNAseq atlas. N.P. supervised the study, provided instrumentation and reagents, and contributed to the writing of the manuscript.

Competing Interests Statement

The authors declare no competing interests.

Figures

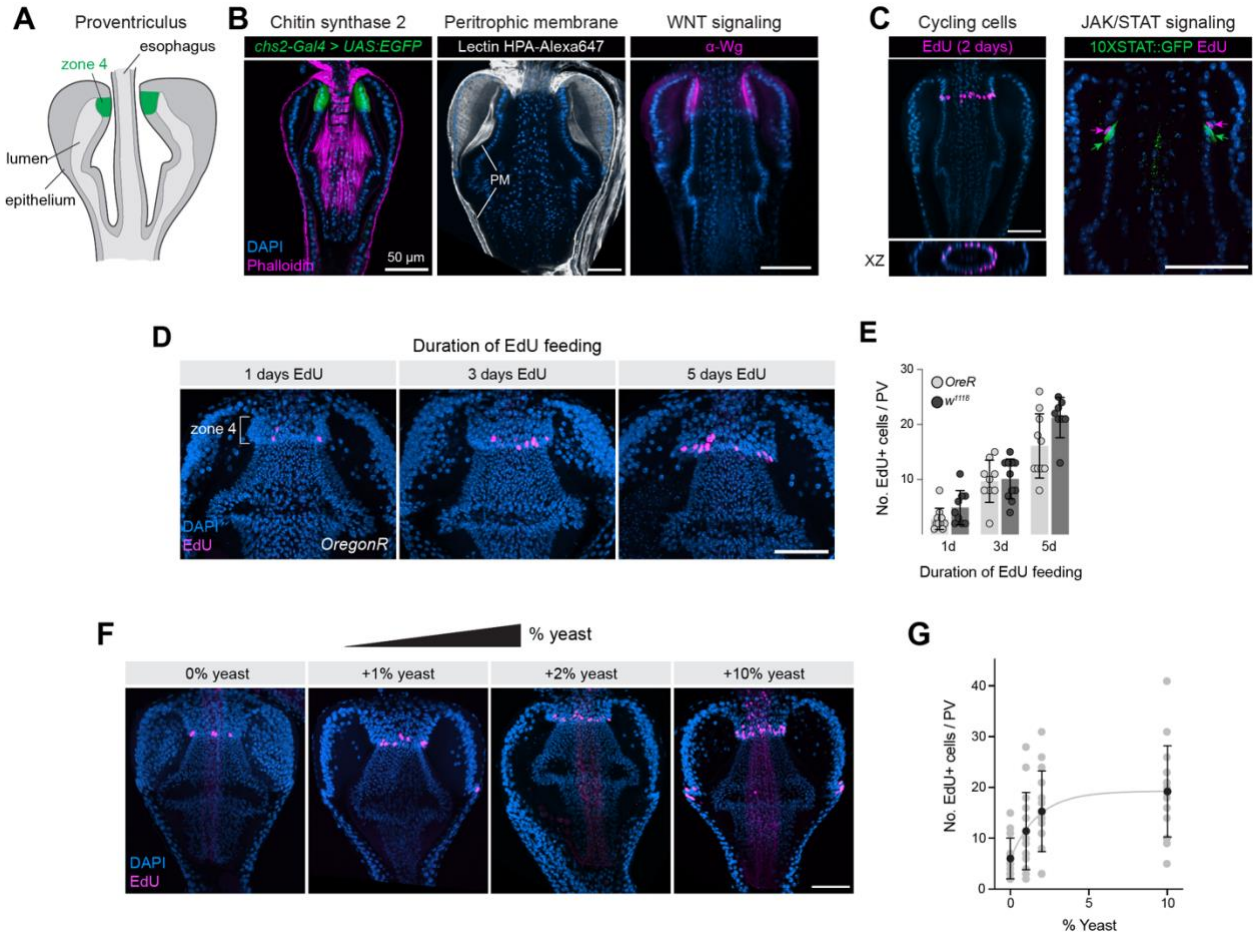

Figure 1. The *Drosophila* proventriculus contains a ring of nutrition-sensitive EdU+ cells located in Zone 4. (A) Schematic of the *Drosophila* proventriculus. Zone 4 is indicated in green. (B) Left: *Chs2-Gal4* is expressed in Zone 4 cells. Representative image is shown from N = 2 independent experiments. Middle: HPA lectin stains the peritrophic membrane (PM). Representative images are shown from > 10 independent experiments. Left: Wg protein is enriched in Zone 4 cells. Confocal z-slices are shown. Representative images are shown from > 5 independent experiments. (C) Left: EdU labeling is enriched in a ring of cells at the posterior of Zone 4. A maximum intensity projection of EdU staining is overlaid on a single z-slice of DAPI staining. Representative image is shown from > 20 independent stainings. Right: EdU+ cells are immediately anterior to cells expressing *10XSTAT:GFP* reporter. Single z-slice is shown. Representative image of a single experiment is shown. (D) The number of EdU+ cells increases with duration of EdU feeding. Maximum intensity projections are shown. (E) Quantification of EdU+ cell numbers at 1, 3, and 5 days of feeding, for two different fly strains, *OregonR* and w^{1118}. N = number of independent proventriculi [1d, 3d, 5d]: *OreR:* 11, 9, 10; w^{1118}: 9, 11, 8. Differences between genotypes at each time point are not significantly different from each other,

tested using the unpaired two-sided t-test with Welch correction. Data is presented as mean +/- SD. (F) The number of EdU+ cells increases as more yeast is added to the food source. Maximum intensity projections are shown. (G) Quantification of the experiment shown in. N = number of independent proventriculi [0%, 1%, 2%, 10%]: 14, 15, 15, 16. Black dots represent mean values, error bars indicate SD. (F) The data were fitted using a one-phase association model, yielding a rate constant K = 0.5689 (95% CI = 0.1639 to 1.463). Anterior is up, scale bar is 50 μm in all images. Source data are provided as a Source Data file.

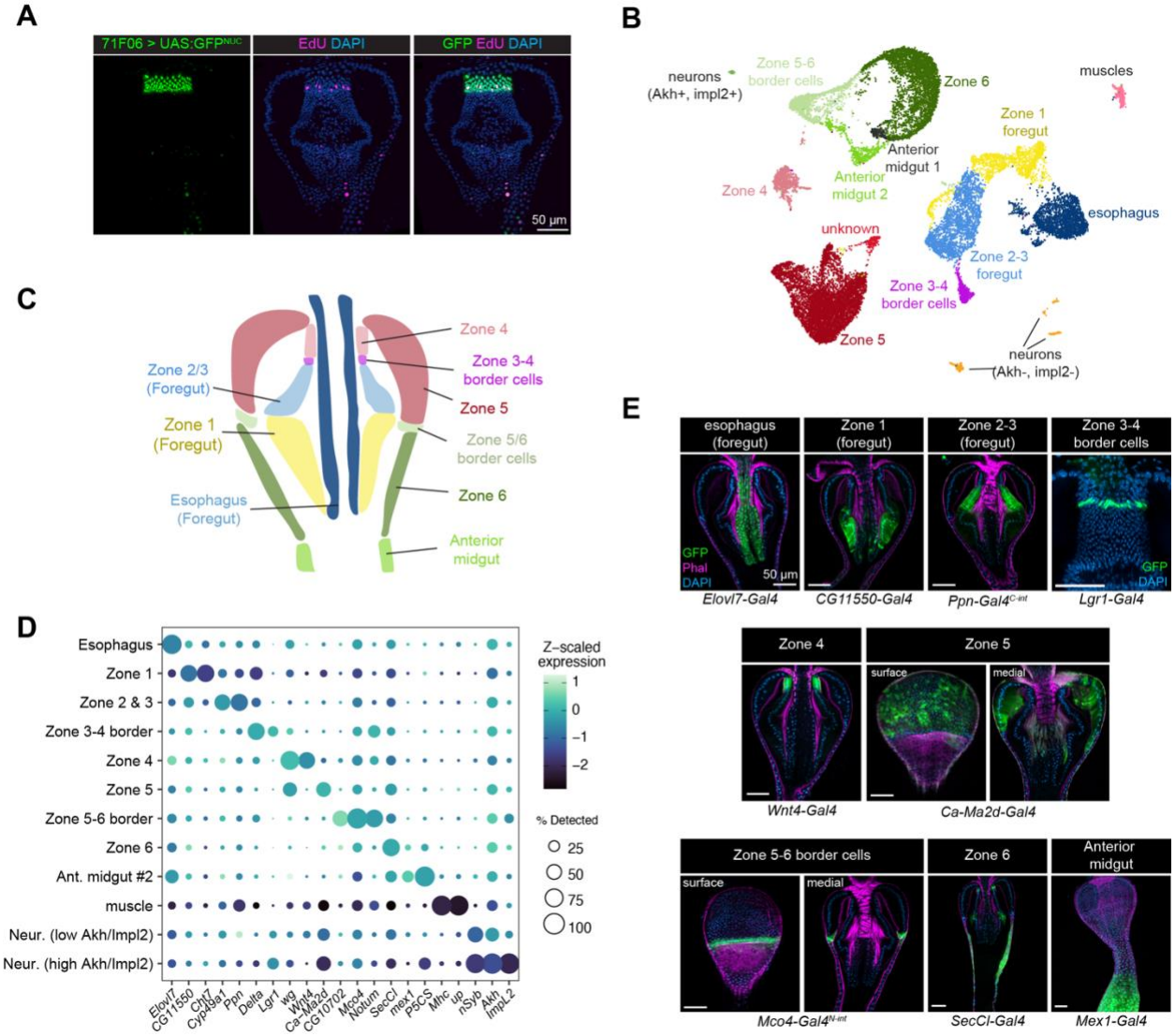

Figure 2. Molecular markers and a single-nuclei atlas for the proventriculus. (A) *71F06-Gal4* drives specific expression in Zone 4 cells, including EdU+ cells. Representative image is shown from > 10 independent stainings. (B) UMAP projection of a single snRNAseq dataset created from 22,332 nuclei, containing 14 clusters representing the major epithelial, muscle, and neuronal cells found in the proventriculus. (C) Schematic of the major epithelial cell types in the proventriculus, corresponding to the clusters identified in (B). (D) Dot plot of selected marker genes for the 12 major clusters identified via snRNAseq; note that two minor clusters ("anterior midgut 1" and "unknown") are excluded from this figure as they could not be clearly linked to *in vivo* cell types. (E) Expression patterns of marker genes for each of the 9 major epithelial cell types in the proventriculus. Anterior is up. Confocal z-slices are shown.

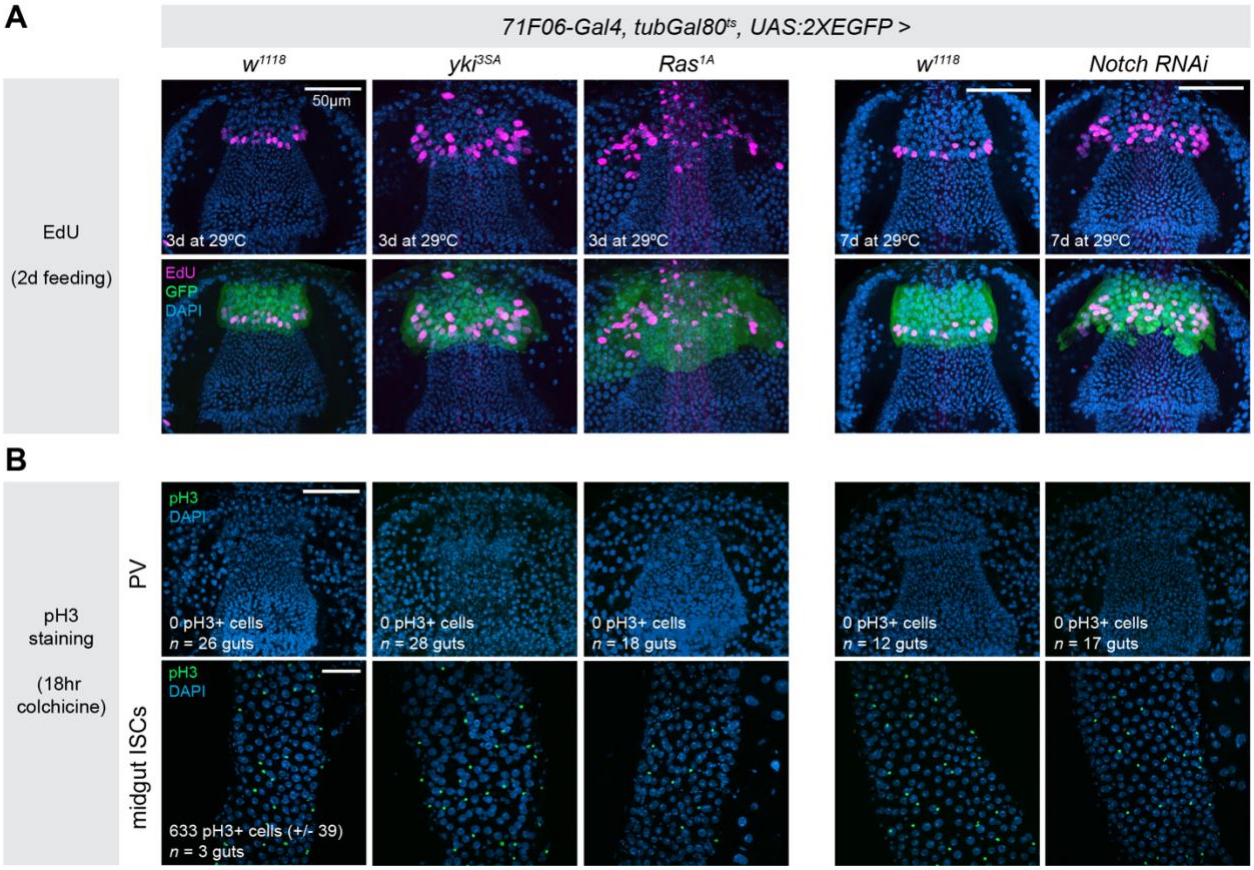

Figure 3. Mitosis is undetectable in Zone 4 cells. (A) Over-expression of *yki*^{3SA}, *Ras*^{1A}, or *Notch-RNAi* in Zone 4 cells increases the number of EdU+ cells and enlarges the size of Zone 4. These data are quantified in Supplementary Figure 4. (B) Zero pH3+ cells were detected in any of the proventriculi examined in any of these genotypes. Flies were fed colchecine for 18 hours prior to dissection to enrich for pH3+ cells. Midgut ISCs from these same guts were included as positive controls, which contained many pH3+ staining in all samples. N = number of independent guts, as listed in the figure. Maximum intensity projections are shown. Anterior is up, scale bar is 50µm in all images. Source data are provided as a Source Data file.

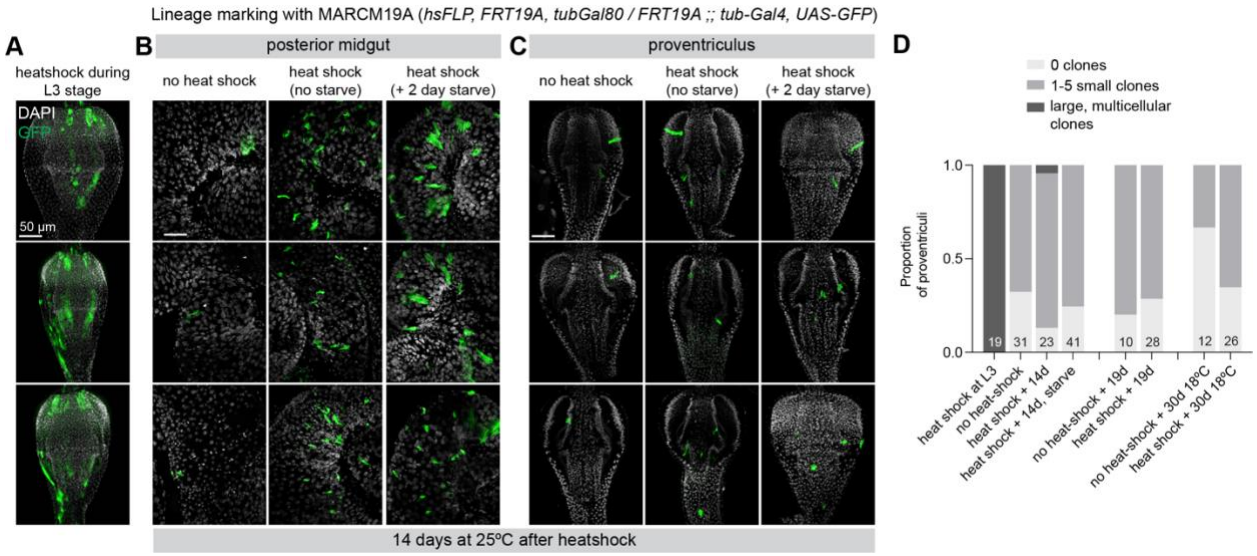

Figure 4. Clonal analysis with MARCM does not label large clones in Zone 4. (A) Positive control for clone induction; clones were induced during the L3 larval stage, leading to large GFP+ clones throughout the proventriculus including in Zone 4. (B) In the posterior midgut, clone induction labels ISCs and their descendants, generating GFP+ clones throughout the midgut. These clones are generally larger when flies endure a 2-day starvation followed by re-feeding. (C) In the proventriculus, small scattered GFP+ cells are detected throughout the tissue, but no discernable enrichment in Zone 4, where EdU+ cells are located. (D) Quantification of several MARCM experiments, with dissection 14 days after clone induction (at 25ºC), 19 days after clone induction (at 25ºC), or 30 days after clone induction (at 18ºC). Maximum intensity projections are shown. N = number of independent guts, as shown in the figure. Data represent multiple examples from single MARCM experiment, with sample sizes given in D. Scale bar is 50µm. Anterior is up. Source data are provided as a Source Data file.

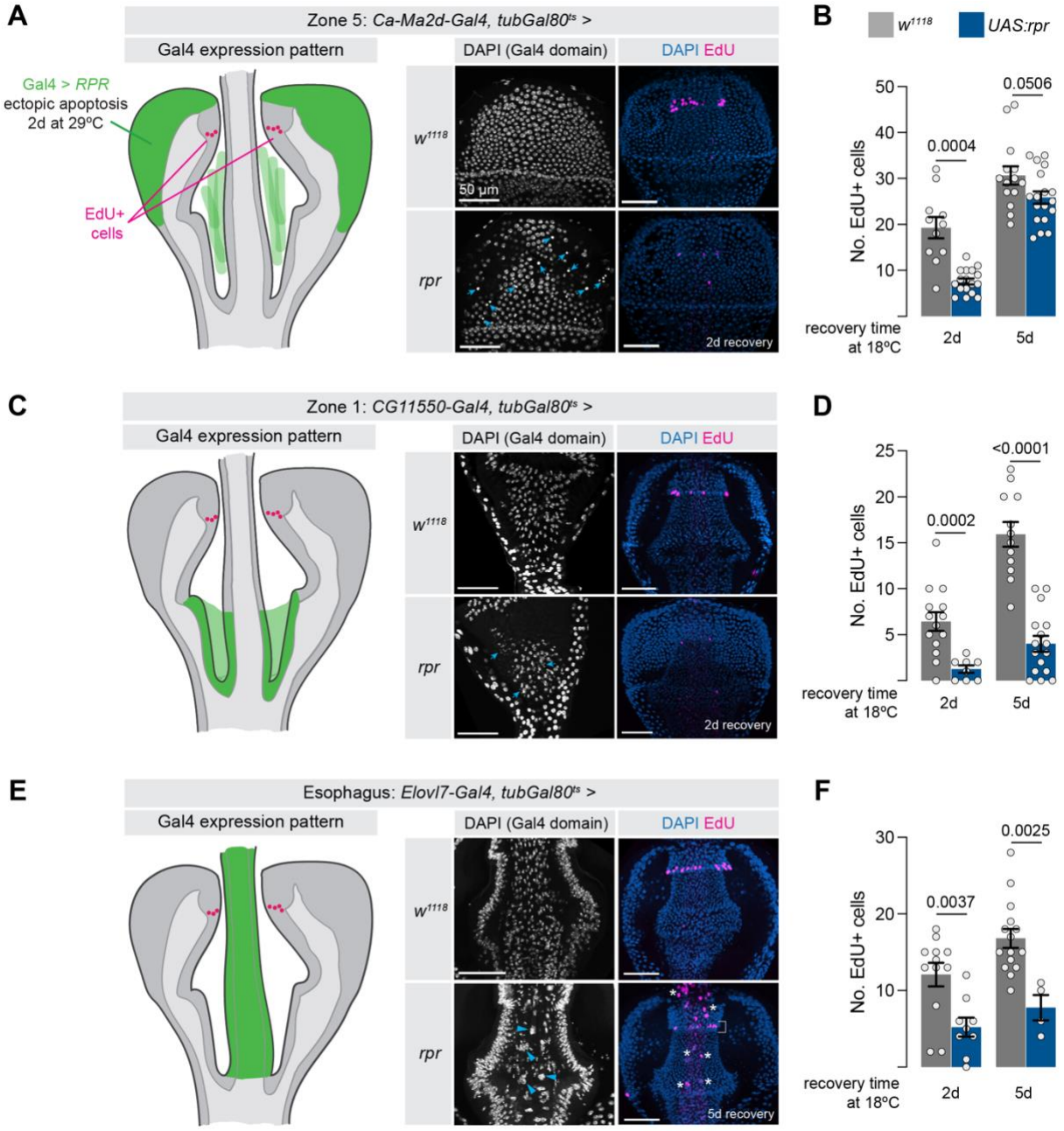

Figure 5. Zone 4 cells do not proliferate to replace cells lost elsewhere in the proventriculus . Tissue damage was induced in three distinct cell types of the proventriculus by over-expressing the pro-apoptotic gene *rpr* for two days, and EdU+ cells were visualized after two and five days of recovery. (A) *rpr* expression in Zone 5, using *Ca-Ma2d-Gal4*, causes a decrease in EdU+ cells after both two and five days. Blue arrows indicate pyknotic nuclei indicative of cell death. (B) Quantification of experiment shown in (A) N = number of independent proventriculi [2d, 5d]: w^{1118}: 11, 14; *rpr*: 17,18. (C) *rpr* expression in Zone 1, using *CG11550-Gal4,* causes a decrease in EdU+ cells after both two and five days. (D) Quantification of experiment shown in (C). N = number of independent proventriculi [2d, 5d]:

w^{1118}: 14, 12; *rpr*: 8,16. (E) *rpr* expression in the esophagus, using *ELOVL7-Gal4*, leads to decreased EdU+ cells in Zone 4, and endoreplication in esophageal cells. White bracket indicates EdU+ signal in Zone 4, blue arrowheads and white asterisks indicate large, EdU+ nuclei in the esophagus itself. (F) Quantification of experiment shown in (E). N = number of independent proventriculi [2d, 5d]: *w^{1118}:* 12, 15; *rpr*: 9,4. Statistical tests in B, D, and F are two-sided unpaired t-tests, with Welch's correction for unequal variances for the 2d tests in (B) and (D). Data is presented as mean +/- SEM. Anterior is up. Scale bar is 50µm in all images. Source data are provided as a Source Data file.

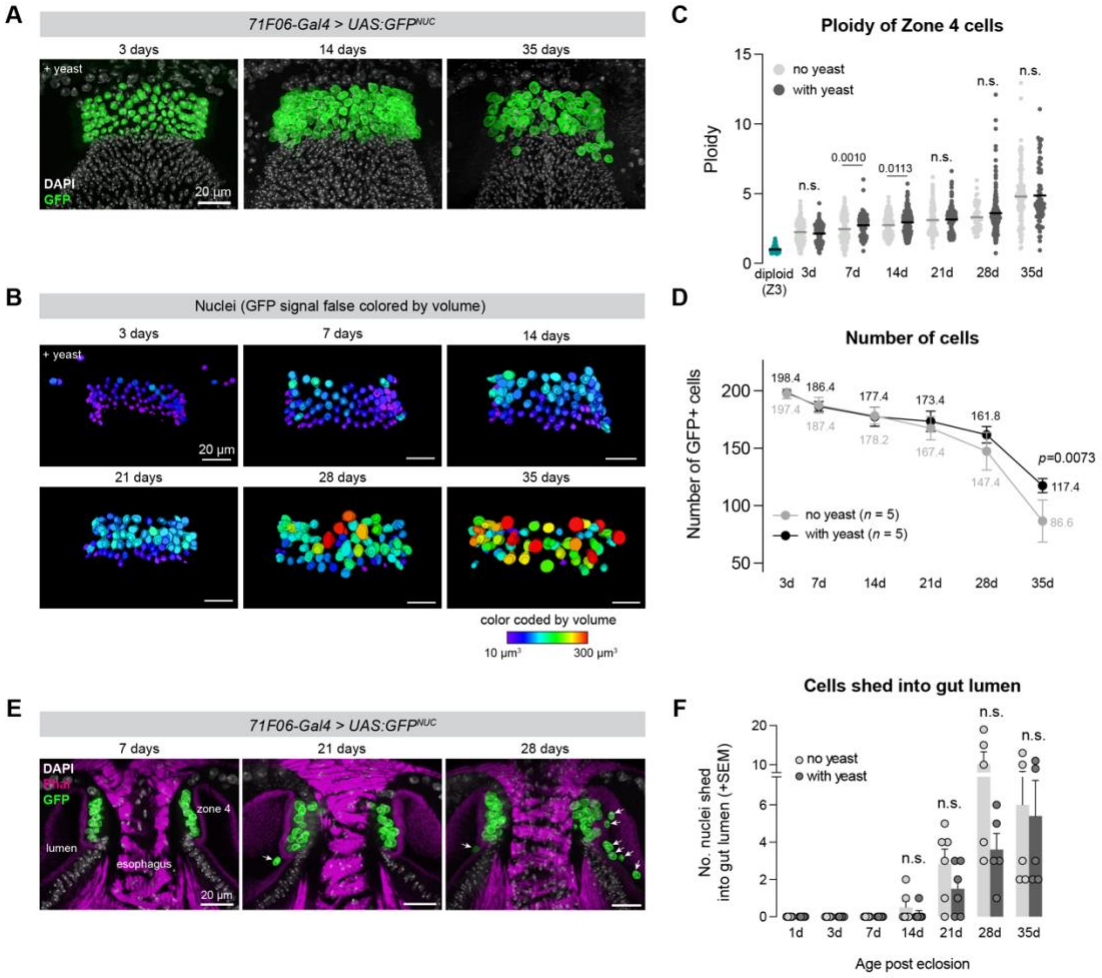

Figure 6. Zone 4 ploidy increases over the fly lifespan, while cells are continually lost into the gut lumen during aging. (A) Time-course of nuclear morphology of the lifespan of the fly, from three days to 35 days post-eclosion. Nuclear-localized GFP was expressed in Zone 4 using *71F06-Gal4*, and flies were provided with or without supplemental yeast powder. (B) Nuclei false-colored by volume. (C) Quantification of ploidy of Zone 4 nuclei, normalized to diploid cells nuclei from Zone 3 cells in the same images. Each dot represents a single nuclei, and lines indicate mean. Ploidy increases throughout the lifespan of a fly, and is signficantly higher in yeast-fed flies at the 7d and 14d time points. Statistical tests are two-sided unpaired t-test, with Welch's correction for unequal variance for the 7d and 28d timepoints; "n.s." = not significantly different. N = number of nuclei measured (no yeast, with yeast): diploid: 102, 3d: 244, 217, 7d: 206, 198, 14d: 174, 228; 21d: 176, 175; 28d: 52, 168; 35d: 108, 78. Repeated measurements were made on nuclei from N = 5 independent proventriculi, except for N = 6 for 14d yeast sample and N = 2 for 28D no yeast sample. (D) The number of Zone 4 cells steadily decreases throughout between 3 days and 35 days post-eclosion, and decreases faster in the absence of yeast powder. Data are shown as mean +/- SEM. N = 5 independent proventriculi per datapoint. Statistical tests were two-sided unpaired t-tests. (E) GFP+ nuclei are consistently observed shed into the lumen adjacent to Zone 4 (F) Quantification of GFP+ cells observed in the lumen at each time point. Data are shown as mean +/- SEM. N = 5 independent

proventriculi per datapoint except N = 6 for 14d and 21d samples, and for 3d + yeast sample. Statistical tests were unpaired t-tests. Source data are provided as a Source Data file.

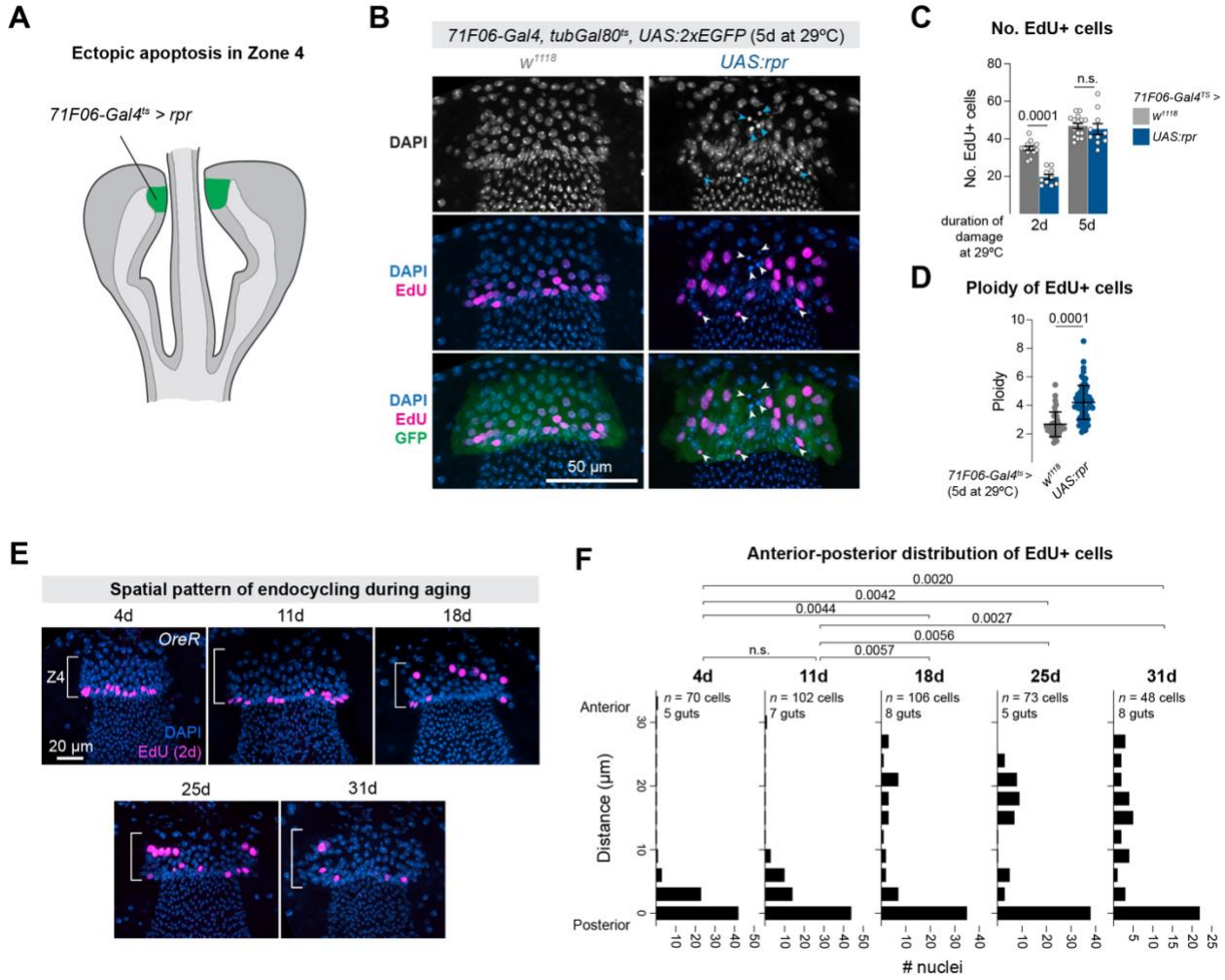

Figure 7. Loss of cells from Zone 4 induces nearby endocycling. (A) *71F06-Gal4^{ts} > rpr* drives apoptosis in Zone 4, for either two or five days. (B) Top row: pycnotic nuclei in Zone 4 indicate cell death (arrowheads). Middle and bottom rows: following tissue damage, EdU+ cells in Zone 4 appear larger are located throughout the tissue rather than enriched at the posterior of Zone 4. Images show tissues after 5d of *rpr* expression. (C) The number of EdU+ cells decreases after two days or *UAS:rpr* expression, but recovers to wildtype levels after five days of damage. N = number of independent proventriculi (*w^{1118}*, *rpr*): 2d: 13, 10; 5d: 15, 10). Mean and SEM are shown. Statistical tests are two-way unpaired t-tests. (D) The ploidy of EdU+ cells is increased following tissue damage in Zone 4. N = number of EdU+ nuclei scored: *w^{1118}*: 39; *UAS:rpr:* 79, repeated measurements from 3 independent *w^{1118}* proventriculi and 6 *UAS:rpr* proventriculi. Mean +/- SD are shown. Statistical test is two-way unpaired t-test with Welch correction. (E) Spatial pattern of EdU+ cells in Zone 4 in aging flies. In younger flies (4d and 11d old), EdU+ cells are restricted to the posterior edge of Zone 4, whereas in older flies (18d, 25d, 31d), EdU+ cells are found throughout more anterior portions of Zone 4. (F) Histograms of the distance of EdU+ nuclei from the posterior edge of the tissue. N = number of EdU+ nuclei and independent proventriculi, as shown in the figure. Statistical tests are Krustal-Wallis tests. Source data are provided as a Source Data file.

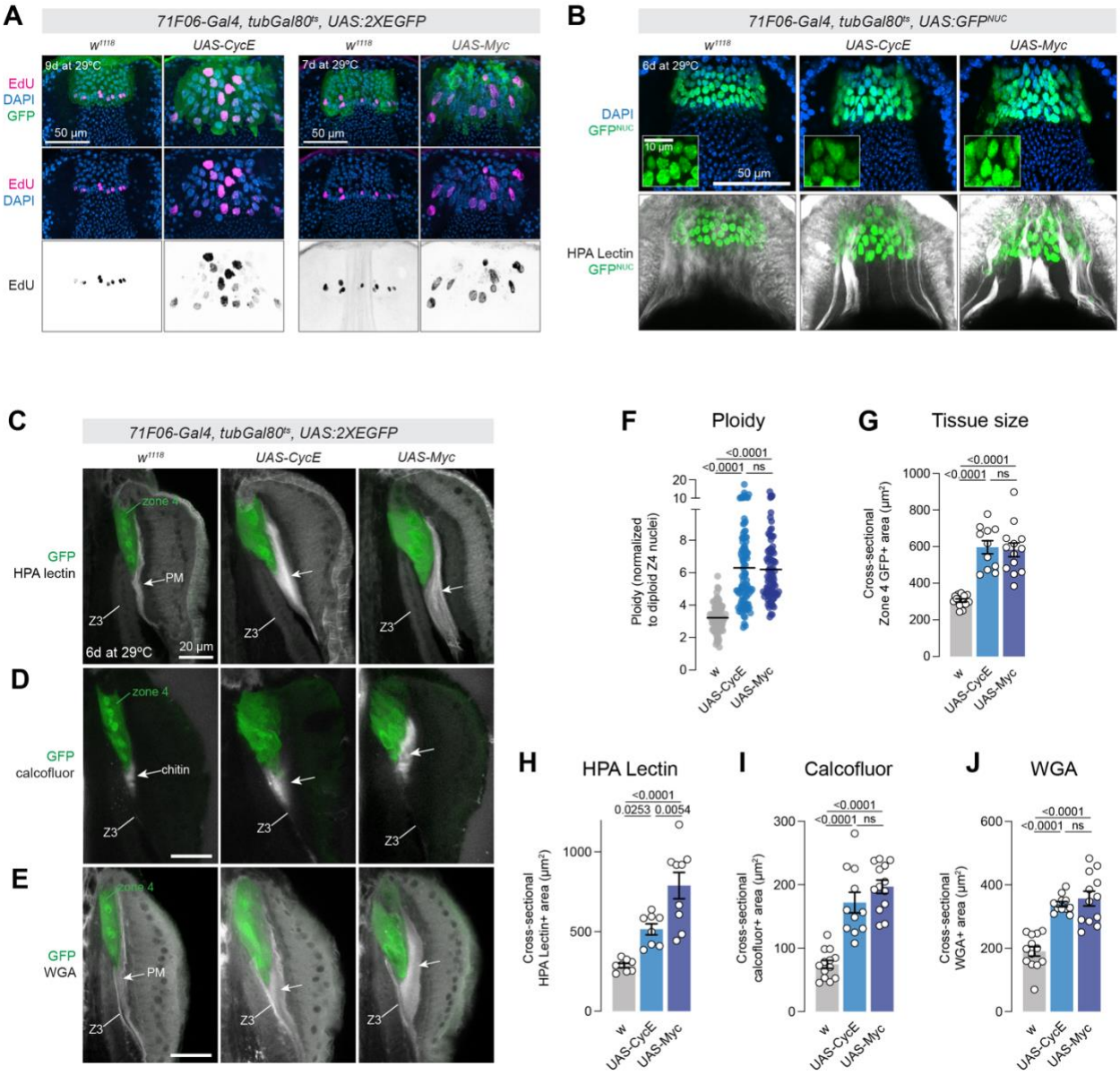

Figure 8. Increased endocycling in Zone 4 cells leads to increased peritrophic membrane synthesis in the proventriculus (A) Over-expression of *CycE* (left) or *Myc* (right) in Zone 4 increases endocycling and nuclear size. Representative images from a single experiment are shown. (B) *71F06-Gal4^{ts}* > *CycE* or *Myc* increases nuclear size (top) and altered peritrophic membrane synthesis. Insets show increased magnification. (C-E) *71F06-Gal4^{ts} CycE* or *Myc* leads to increased tissue size, and (C) increased HPA lectin staining; (D) increased calcofluor staining, and (E) increased amount of WGA staining. Images are maximum intensity projections of 3-4 z-slices. Z3 = zone 3, which includes a chitinous border that is distinct from peritrophic membrane. (F) Quantification of ploidy for flies shown in (B). Each dot represents a nucleus, bar represents the mean. N = 85 *w^{1118}* nuclei from 4 proventriculi, 102 *CycE* nuclei from 5 proventriculi, and 88 *Myc* nuclei from 4 proventriculi. Statistical test is a one-way ANOVA with Tukey's multiple comparison test. (G) Quantification of tissue size. In G-J, each dot represents

the average of two measurements per proventriculus. N = number of independent proventriculi: w^{1118} = 13, *CycE* = 11, *Myc* = 13. Statistical test is a one-way ANOVA with Tukey's multiple comparison test. (H) Quantification of HPA lectin staining. Number of independent proventriculi is 8 w^{1118}, 8 *CycE*, and 9 *Myc.* Statistical test is a one-way ANOVA with Tukey's multiple comparison test. (I) Quantification of the area of calcofluor-positive material. Number of independent proventriculi is 13 w^{1118}, 11 *CycE*, and 13 *Myc.* Statistical test is a one-way ANOVA with Tukey's multiple comparison test. (J) Quantification of the area of WGA-positive material. Number of independent proventriculi is 13 w^{1118}, 11 *CycE*, and 12 *Myc.* Statistical test is a one-way ANOVA with Tukey's multiple comparison test. Data in G-J are shown as mean +/- SEM. Source data are provided as a Source Data file.

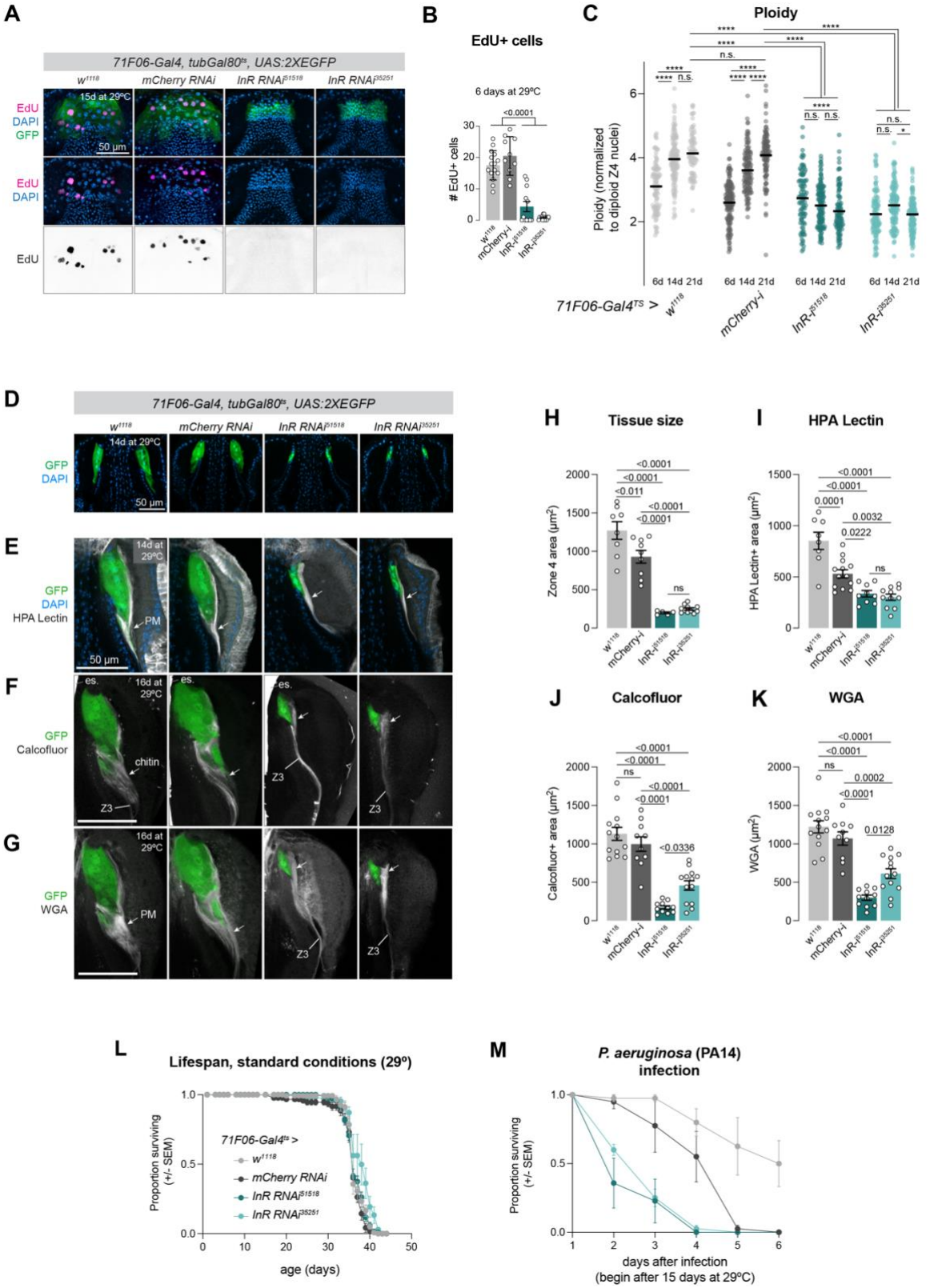

(Caption on next page)

Figure 9. **Blocking endocycling in Zone 4 reduces peritrophic membrane synthesis.** (A) *71F06-Gal4*^{ts} > *InR-RNAi* reduces EdU incorporation and tissue size. (B) Quantifcation of A. Number of independent proventriculi: 15 *w*^{1118}, 10 *mCherry-RNAi*, 12 *InR-RNAi*^{51518}, 13 *InR-RNAi*^{35251}. Statistical test is Ordinary one-way ANOVA. Data is shown as mean +/- SD. (C) *InR-RNAi* reduces ploidy. Bars represent mean. N = number of nuclei (6d, 14d, 21d) = *w*^{1118}*:* 92, 120, 76; *mCherry-RNAi:* 152, 129, 112, 95; *InR-RNAi*^{51518}: 95, 135, 98; *InR-RNAi*^{35251}: 105, 121, 120. N = number of independent guts (6d, 14d, 21d): *w*^{1118}*:* 4, 4, 3; *mCherry-RNAi:* 4, 4, 4; *InR-RNAi*^{51518}: 3, 4, 4; *InR-RNAi*^{35251}: 4, 4, 4. Statistical test: one-way ordinary ANOVA test with Tukey's multiple comparison test. **** $p < 0.0001$; * $p = 0.0134$. (D) *InR-RNAi* reduces tissue size. (E-G) *InR-RNAi* reduces peritrophic membrane synthesis: (E) HPA lectin, (F) calcofluor, and (G) WGA. Z3 = zone 3. (H) Quantification of tissue size. In H-K, each dot represents the average of two measurements per proventriculus. N = number of independent proventriculi = *w*^{1118}: 8, *mCherry-RNAi*: 9, *InR-RNAi*^{51518}*:* 5, *InR-RNAi*^{35251}: 11. Statistical test: one-way ANOVA with Tukey's multiple comparison test. Data in H-M is presented as mean +/- SEM. (I) Quantification of E. N = number of independent proventriculi = *w*^{1118}: 8, *mCherry-RNAi:* 13, *InR-RNAi*^{51518}: 9, *InR-RNAi*$^{35251:}$ 11. Statistical test: one-way ANOVA with Tukey's multiple comparison test. (J) Quantification of F. N = number of independent proventriculi = *w*^{1118}: 13, *mCherry-RNAi*: 10, *InR-RNAi*^{51518}*:* 11 *InR-RNAi*^{35251}*:* 13. Statistical test: one-way ANOVA with Tukey's multiple comparison test. (K) Quantification of G. N = number of independent proventriculi = *w*^{1118}*: 13, mCherry-RNAi*: 10, *InR-RNAi*^{51518}*:* 11, *InR-RNAi*^{35251}: 13. Statistical test: one-way ANOVA with Tukey's multiple comparison test. (L) Lifespan is not affected by *InR-RNAi*. N = number of flies: *w* = 134; *mCherry-RNAi* = 95; *InR-RNAi*^{51518} = 128; *InR-RNAi*^{35251} = 58; 15 flies per vial. (M) *InR-RNAi* leads to increased susceptibility to *PA14*. N = number of flies: *w* = 40; *mCherry-RNAi* = 40; *InR-RNAi*^{51518} = 38; *InR-RNAi*^{35251} = 40; 9-10 flies per vial. Data in D-K represent single experiments; L was repeated once with similar results. Source data are provided as a Source Data file.

Supplementary Figures:

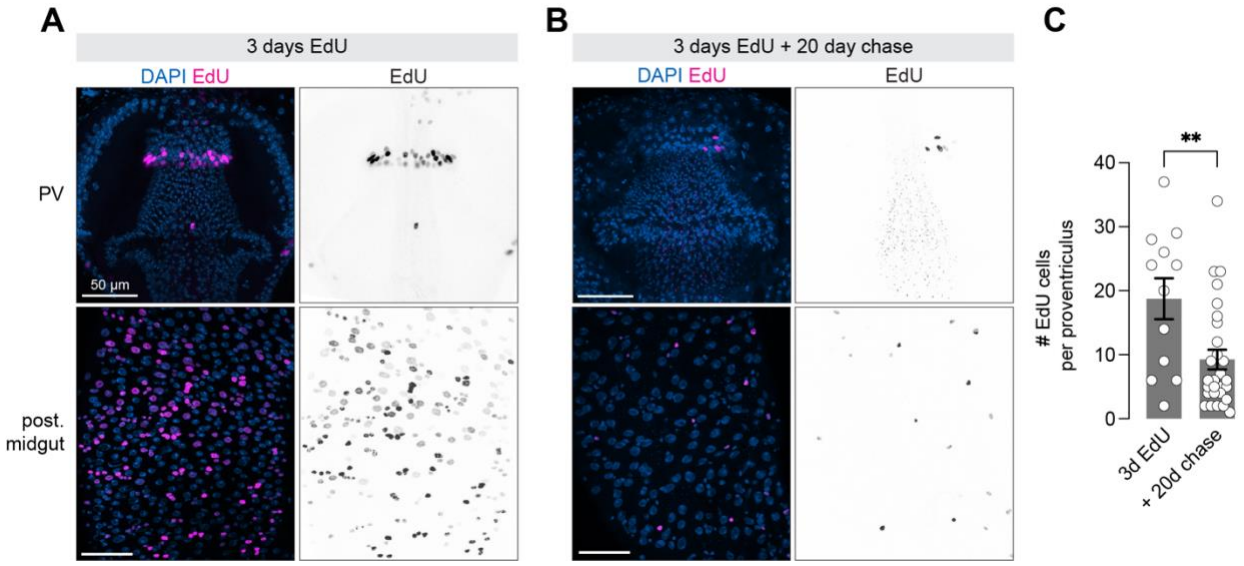

Supplementary Figure 1. EdU+ cells in Zone 4 cycle continuously. (A) After 3 days of EdU feeding, a ring of labeled cells is visible at the posterior edge of Zone 4, as well as in the ISCs and enterocytes of the midgut. (B) Following a 20 day chase period, a reduction of EdU+ cells is visible in both Zone 4 cells and in the midgut, where continual cycling has diluted out the original EdU pulse. (C) Quantification of data shown in A-B. N = 3d: 9 independent proventriculi, 20d chase: 22 independent proventriculi. Statistical test is an unpaired t-test; ** = 0.0024. “PV” = proventriculus. “post-midgut” = posterior midgut.

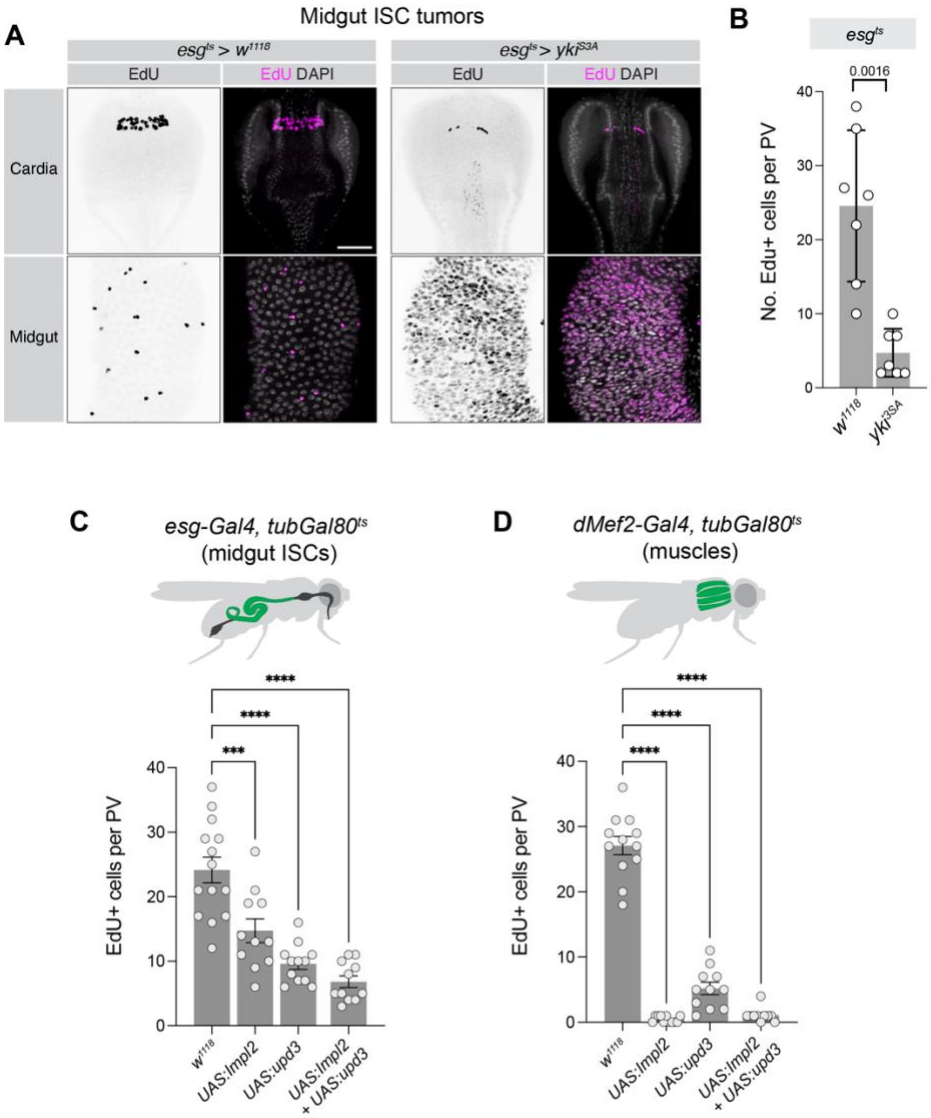

Supplementary Figure 2. Systemic reduction in insulin signaling reduces the number of EdU+ cells in the proventriculus. (A) Tumors in midgut ISCs (driven by *esg-Gal4*^{ts} > *yki*^{3SA}) cause a reduction in EdU+ cells in the proventriculus. Note that *esg-Gal4* is not expressed in the proventriculus. Anterior is up, scale bar is 50 µm. (B) Quantification of the experiment shown in (A). N = 7 independent proventriculi. Statistical test is Welch's t-test. (C) Over-expression of insulin-antagonists *ImpL2, upd3,* or a combination of both from the ISCs (*esg-Gal4*) leads to a reduction in EdU+ cells. N = independent proventriculi: *w*^{1118} = 14; *UAS:Impl2* = 11; *UAS:upd3* = 12; *UAS:Impl2+UAS:upd3* = 11. Statistical tests are one-way ANOVA; *** p = 0.0003; **** p < 0.0001. (D) Over-expression of insulin-antagonists *ImpL2, upd3,* or a combination of both from muscles using *dMef2-Gal4* leads to a reduction in EdU+ cells. N = independent proventriculi: *w*^{1118} = 12; *UAS:Impl2* = 11; *UAS:upd3* = 11; *UAS:Impl2+UAS:upd3* = 10. Statistical tests are one-way ANOVA; **** p < 0.0001.

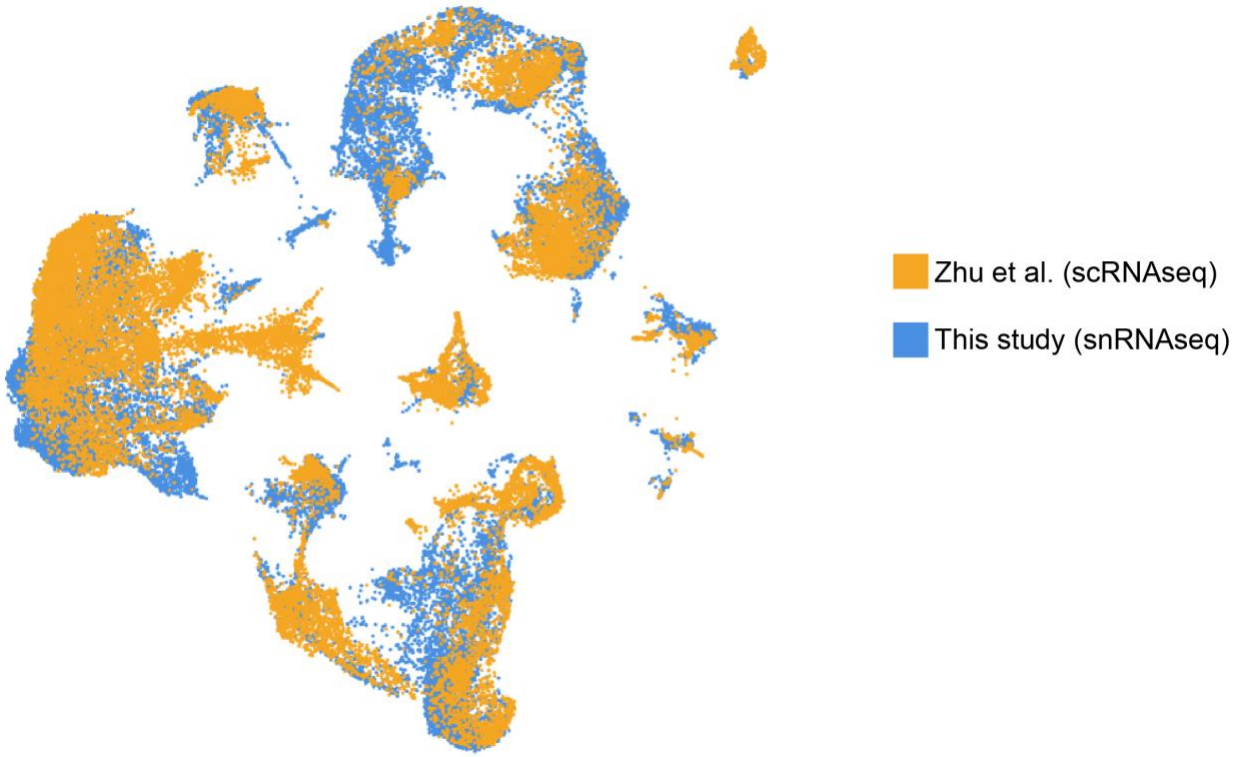

Supplementary Figure 3. Merged UMAP projection of two single cell atlases of the proventriculus. Data from the snRNAseq atlas presented in this manuscript and scRNAseq data from Zhu *et al.* (2024) [main referenance 25] were bioinformatically pooled and re-analyzed into a single dataset.

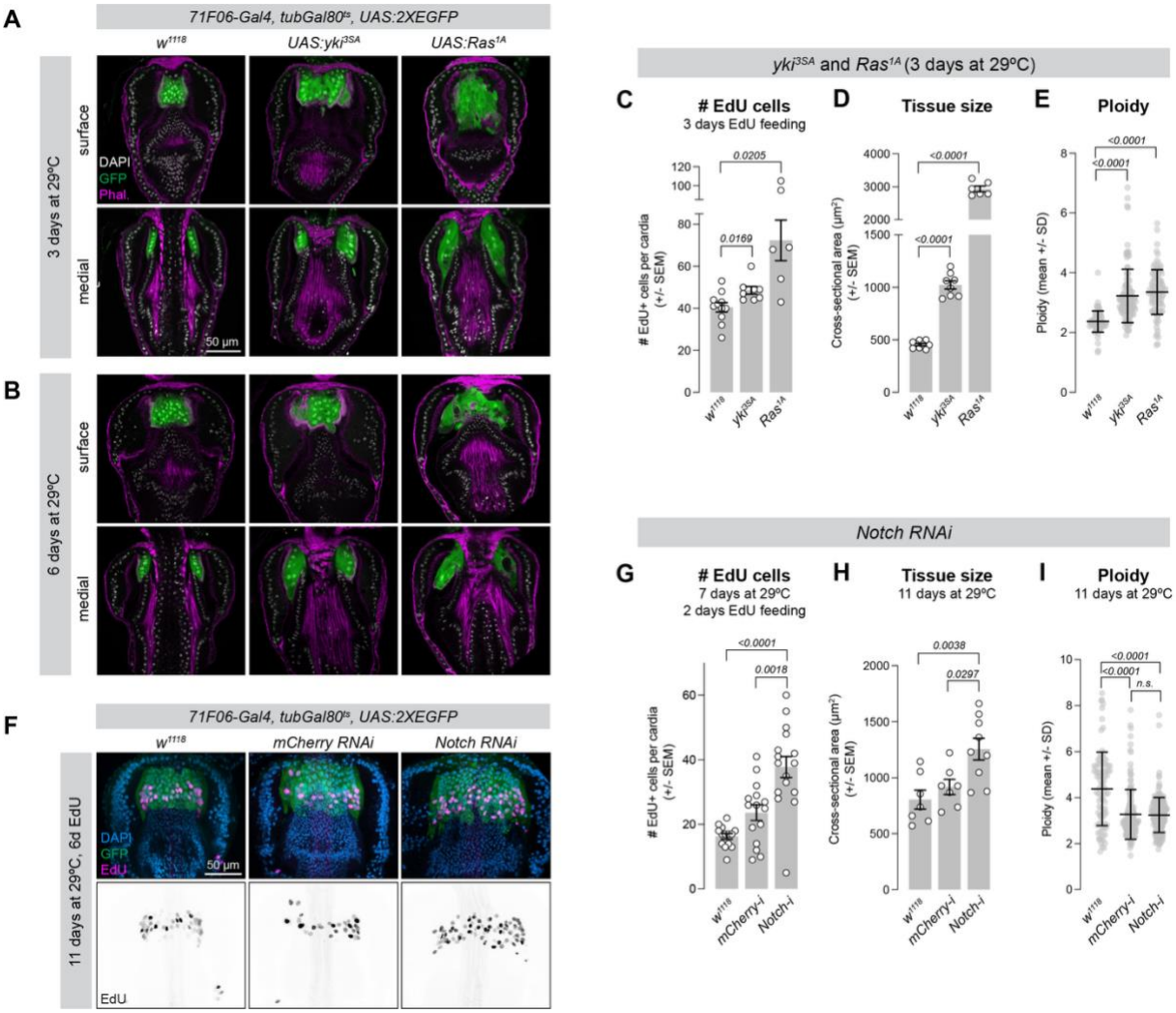

Supplementary Figure 4. Additional characterization of *yki^{3SA}*, *Ras^{1A}*, and *Notch-RNAi* phenotypes in proventriculus Zone 4 cells. (A-B) Ectopic expression of oncogenes *yki^{3SA}* or *Ras^{1A}* in Zone 4 cells of the proventriculus for either (A) three days or (B) six days leads to tissue enlargement, yet no GFP+ cells are visible outside of Zone 4. (C) *71F06-Gal4^{ts} > yki^{3SA}* or *Ras^{1A}* leads to increased number of EdU+ cells. N = independent proventriculi: *w^{1118}* = 11; *yki^{3SA}* = 8; *Ras^{1A}* = 6. Statistical test is two-tailed unpaired t-test. (D) *71F06-Gal4^{ts} > yki^{3SA}* or *Ras^{1A}* leads to increased tissue size, measured as cross-sectional area at the tissue midpoint. Each value represents the average of two measures per proventriculus, on either side of the esophagus. N = independent proventriculi: *w^{1118}* = 9; *yki^{3SA}* = 8; *Ras^{1A}* = 6. Statistical test is two-one-way ANOVA with Tukey's multiple comparison test (E) *71F06-Gal4^{ts} > yki^{3SA}* or *Ras^{1A}* leads to increased ploidy. Each point represents a single nucleus; N = number of nuclei: *w^{1118}* = 76; *yki^{3SA}* = 110; *Ras^{1A}* = 98, measured from 4 independent proventriculi. (F) *71F06-Gal4^{ts} > Notch-RNAi* leads to increased tissue size and increased number of EdU cells. (G) Number of EdU+ cells in *71F06-Gal4^{ts} > Notch-RNAi* flies is significantly increased compared to controls. N = independent proventriculi: *w^{1118}* = 14; *mCherry-RNAi* = 15; *Notch-RNAi* = 16. Statistical test is

one-way ANOVA with Tukey's multiple comparison test. (H) *71F06-Gal4*^{ts} > *Notch-RNAi* causes increased Zone 4 tissue size. N = independent proventriculi: *w*^{1118} = 7; *mCherry-RNAi* = 7; *Notch-RNAi* = 9. Statistical test is one-way ANOVA with Tukey's multiple comparison test. (I) Ploidy is not increased in *71F06-Gal4*^{ts} > *Notch-RNAi,* and does not significantly differ from *mCherry-RNAi* controls. N = number of nuclei: *w*^{1118} = 144; *mCherry-RNAi* = 92; *Notch-RNAi* = 201. N = number of independent proventriculi: *w*^{1118} = 5; *mCherry-RNAi* = 7; *Notch-RNAi* = 7. Statistical test is one-way ANOVA with Tukey's multiple comparison test.

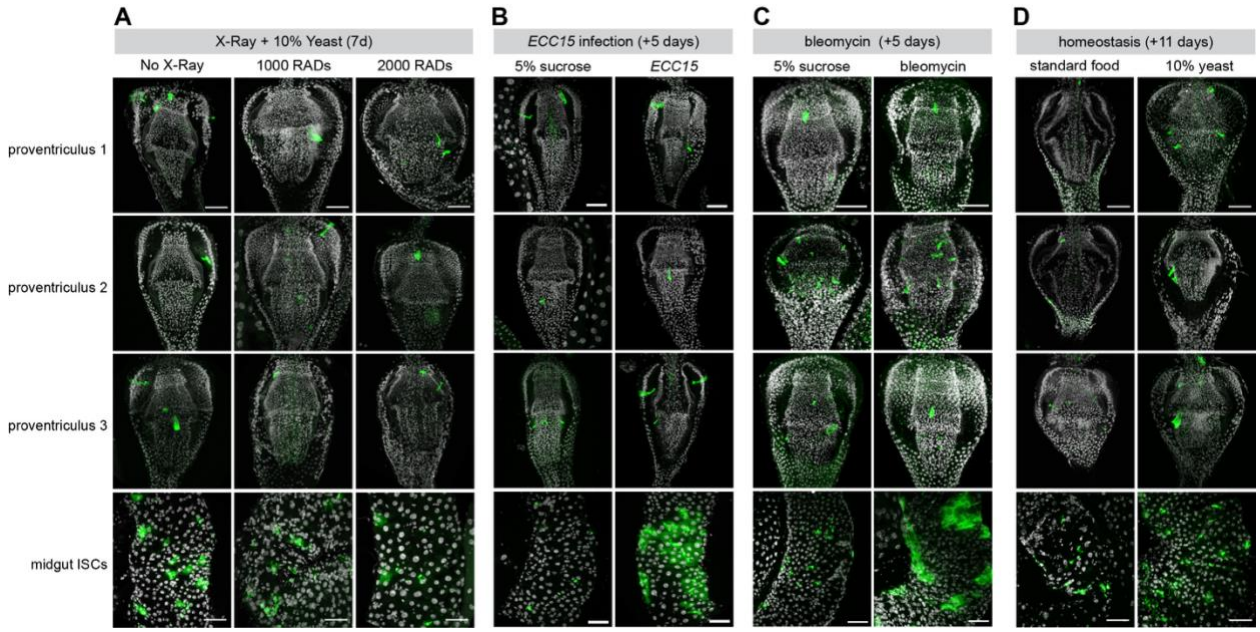

Supplementary Figure 5. MARCM analysis in the proventriculus following gut damage. Analysis of MARCM clones in the proventriculus and midgut following a number of perturbations to the gut. Three representative proventriculus images are shown for each condition, from a total sample size between 10 and 23 guts. (A) X-ray damage to entire flies at 1000 or 2000 RADS, examined seven days after damage. (B) Gut damage from *ECC15* bacteria, examined 5 days after damage. (C) Gut damage from bleomycin, examined 11 days after damage. (D) Undamaged guts, fed with food supplemented with 10% yeast. Anterior is up, scale bar is 50μm.

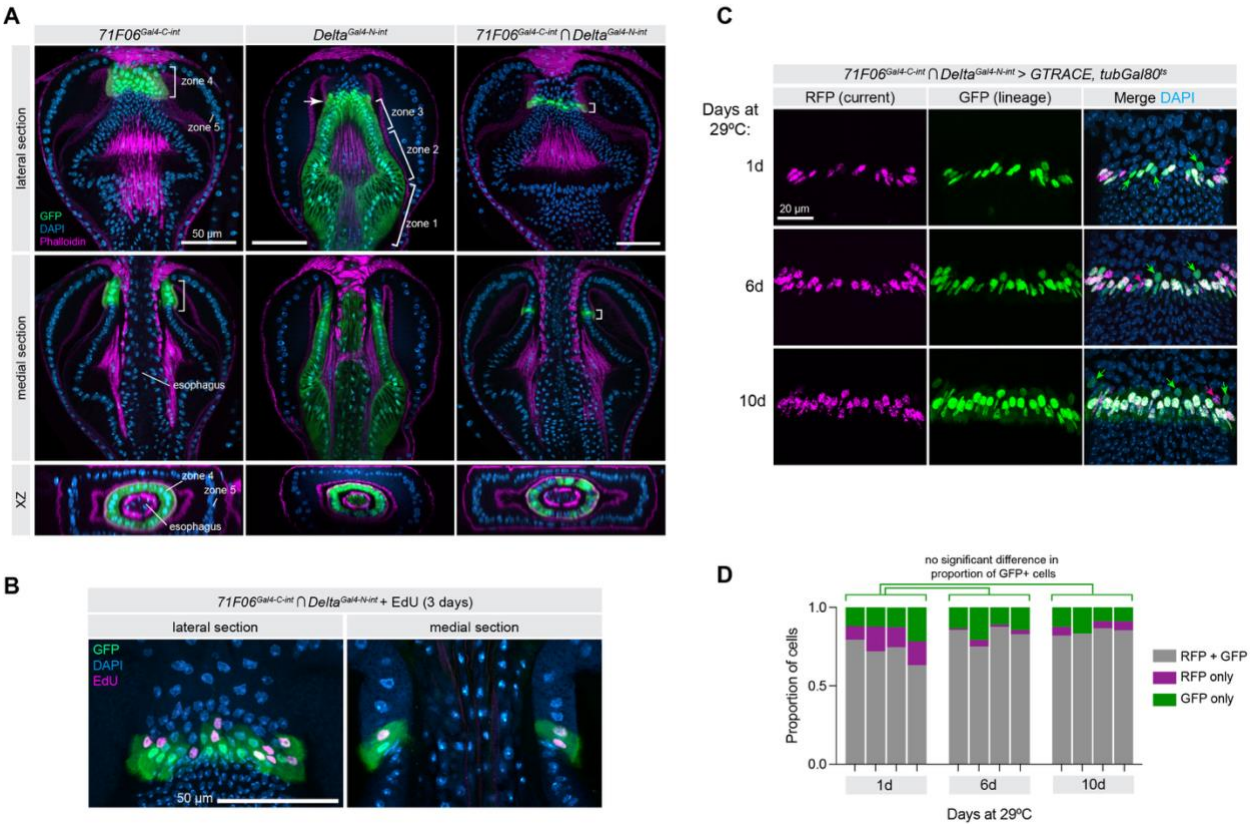

Supplementary Figure 6. Genetic lineage tracing using a highly specific split-intein Gal4 that labels Edu+ cells. (A) Expression pattern of *71F06*$^{Gal4\text{-}C\text{-}int}$, *Delta*$^{Gal4\text{-}N\text{-}int}$, and the intersection of *71F06 ∩ Delta*. (B) *71F06 ∩ Delta* expression largely overlaps with EdU+ cells in Zone 4 cells. (C) Using *71F06 ∩ Delta* to drive the G-TRACE lineage system, with *tubGal80*^{ts} to restrict labeling to the adult stage for the indicated duration. Colored arrows indicate individual cells with either solely GFP (past but not current expression) or RFP (very recently initiated expression.) Anterior is up. (D) Quantification of experiment shown in (C). Each column represents a single proventriculus sample at the indicated time-point. Statistical comparison is calculated as ordinary one-way ANOVA comparing the proportion of GFP-only cells between time-points. N = 4 independent proventriculi at each time point. Statistical test is Kruskal Wallace test, p = 0.5101.

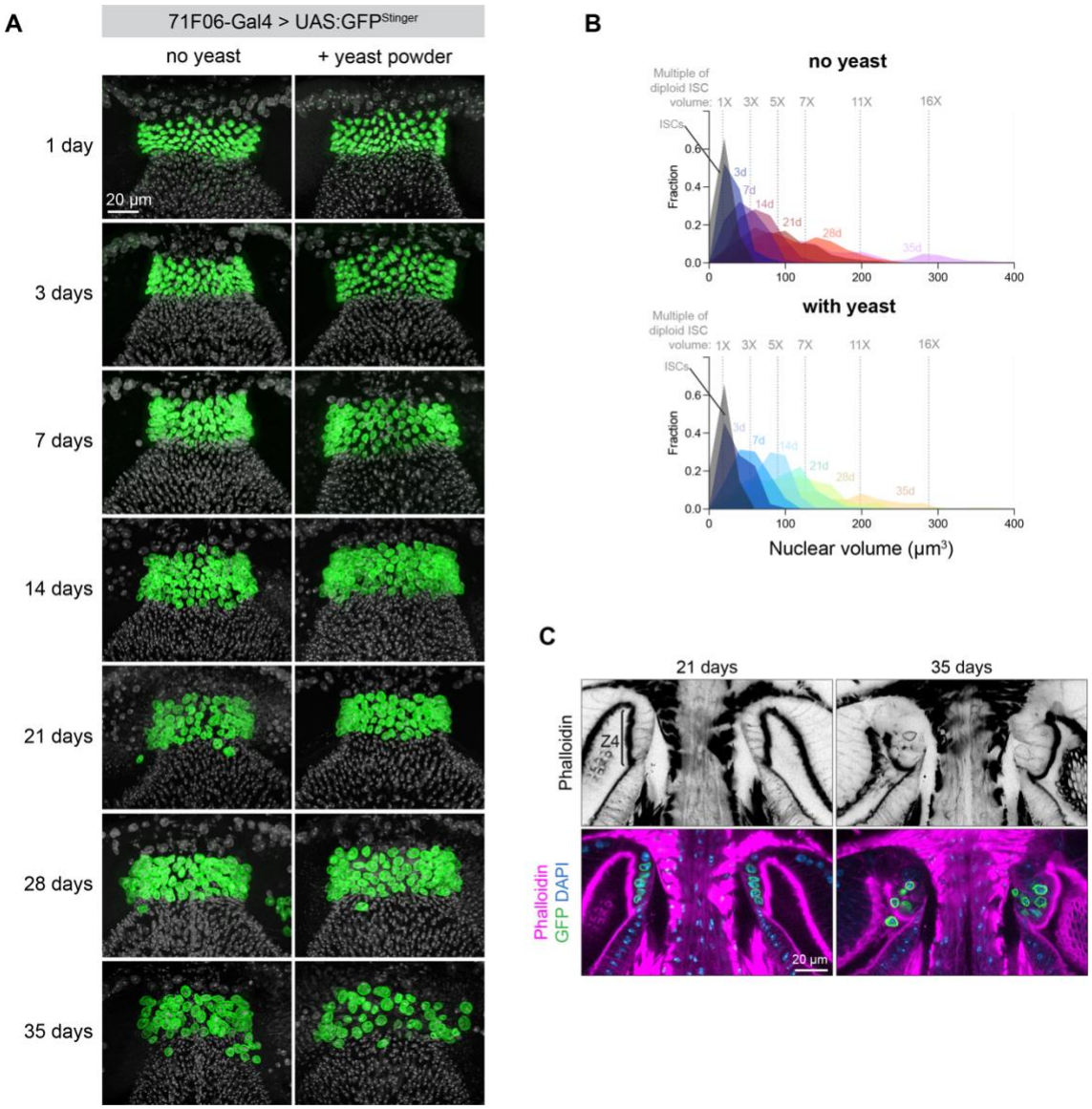

Supplementary Figure 7. Time course analysis of nuclear volume and morphology in Zone 4 cells. (A) Representative images of each time-point for the experiment shown in Figure 7. (B) Histogram of nuclear volume calculated from the data represented in Figure 7. (C) 71F06> Stinger flies aged 21d (left) or 35d (right) and stained for phalloidin, indicating that cells remain mononucleate throughout this time-course. Z4 = zone 4. Anterior is up.

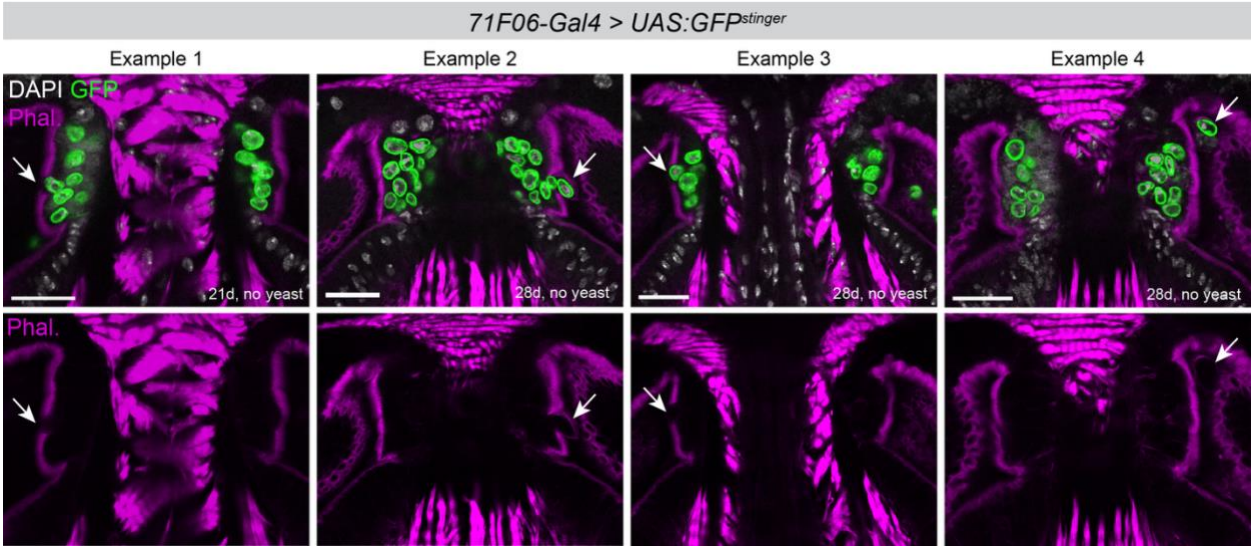

Supplementary Figure 8. Additional examples of Zone 4 nuclei loss into the gut lumen. In aging flies, GFP+ nuclei can be seen shed into the gut lumen from Zone 4. Multiple examples are shown of these nuclei appearing to exit Zone 4 through disruptions in the apical (lumen-facing) surface of Zone 4, visible as loss of phalloidin. Cells are observed at various locations along the anterior-posterior axis of Zone 4. Anterior is up, scale bar is 20μm.

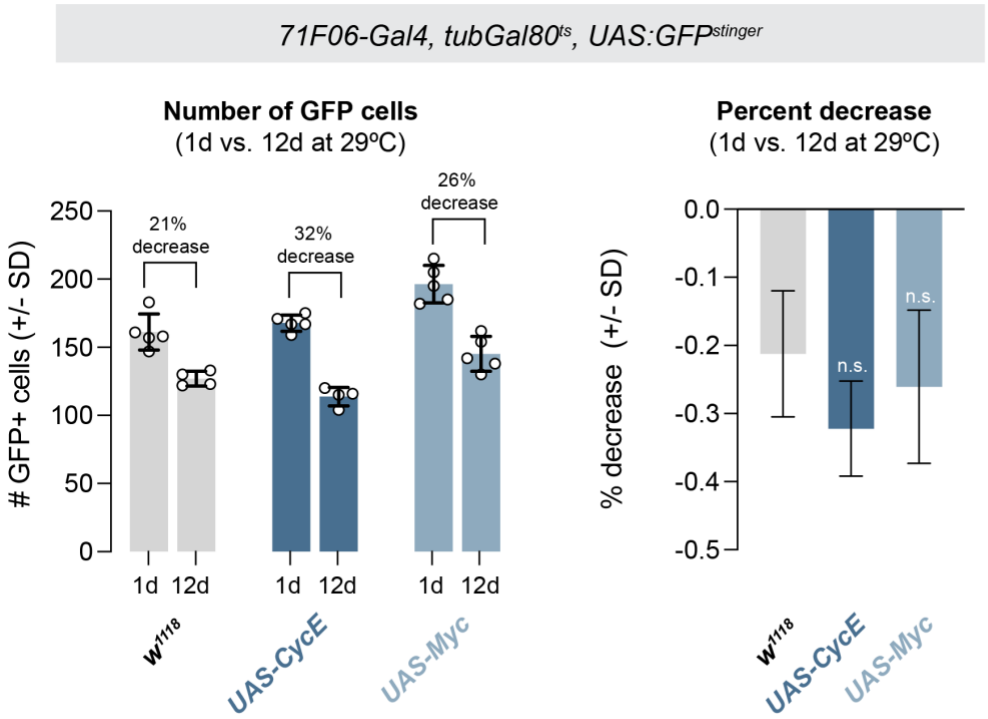

Supplementary Figure 9. Increased endocycling does not enhance cell loss in Zone 4. Left: Cell counts of GFP+ Zone 4 cells after 1 day or 12 days at 29ºC for the indicated genotypes. N = independent proventriculi (1d, 12); w^{1118} = 5, 4; *CycE* = 5, 4; *Myc* = 5,5. Right: the average percentage decrease, calculated from the data shown on the left, was not significantly different between these conditions. Error bars represent standard deviation propagated through the calculation of percentage decrease, and mean differences were compared using a two-way unpaired t-test.

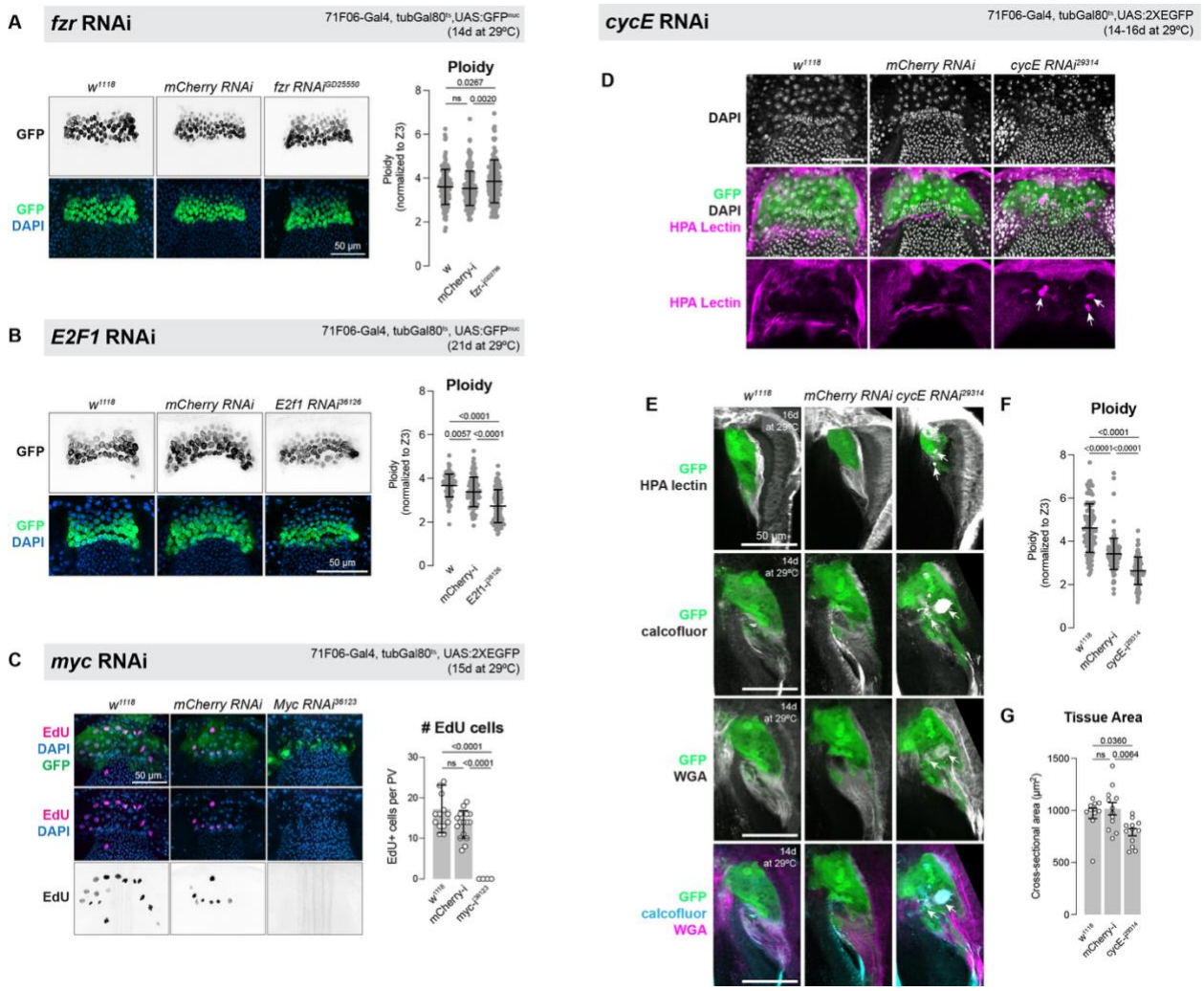

Supplementary Figure 10. RNAi against additional candidates implicated in endocycling. (A) RNAi against *fzr* does not reduce ploidy in Zone 4, and in fact slightly increases cell ploidy. Representative images are shown to the left, quantification of ploidy shown at right. N = number of nuclei: *w* = 153; *mCherry-RNAi* = 180*; fzr-RNAi* = 160. N = number of independent proventriculi = 5. Statistical test is one-way ANOVA with Tukey's multiple test correction. (B) RNAi against *E2F1* significantly reduces ploidy in Zone 4, to a lesser degree than *InR-RNAi.* Representative images are shown to the left, quantification of ploidy shown at right. N = number of nuclei: *w* = 105; *mCherry-RNAi* = 99*; fzr-RNAi* = 124. N = number of independent proventriculi; *w* = 5; *mCherry-RNAi* = 4; *E2F1-RNAi* = 5. Statistical test is one-way ANOVA with Tukey's multiple test correction. (C) RNAi against *myc* abolishes EdU incorporation (right) but also massively disrupts or destroys Zone 4 morphology (left.) (D) Representative images of *71F06-Gal4^{ts} > cycE-RNAi,* demonstrating smaller nuclei (top row) and aggregates of peritrophic membrane, revealed via HPA lectin staining (bottom row, arrows.) (E) RNAi against *cycE* causes aggregates of peritrophic membrane in Zone 4 that stains for HPA lectin, calcofluor, and WGA (arrows). (F) *71F06-Gal4^{ts} > cycE-RNAi* reduces ploidy. N = number of nuclei: *w* = 110;

mCherry-RNAi = 136*; fzr-RNAi* = 79. N = number of independent proventriculi; *w* = 5; *mCherry-RNAi* = 5; *cycE-RNAi* = 4. Statistical test is one-way ANOVA with Tukey's multiple test correction. (G) *71F06-Gal4*^{ts} > *cycE-RNAi* reduces tissue size compared to controls. Each point represents the average of two measurements per proventriculus. N = number of independent proventriculi: *w*^{1118} = 11, *mCherry-RNAi* = 12, *cycE-RNAi* = 12. Statistical test is one-way ANOVA with Tukey's multiple test correction.

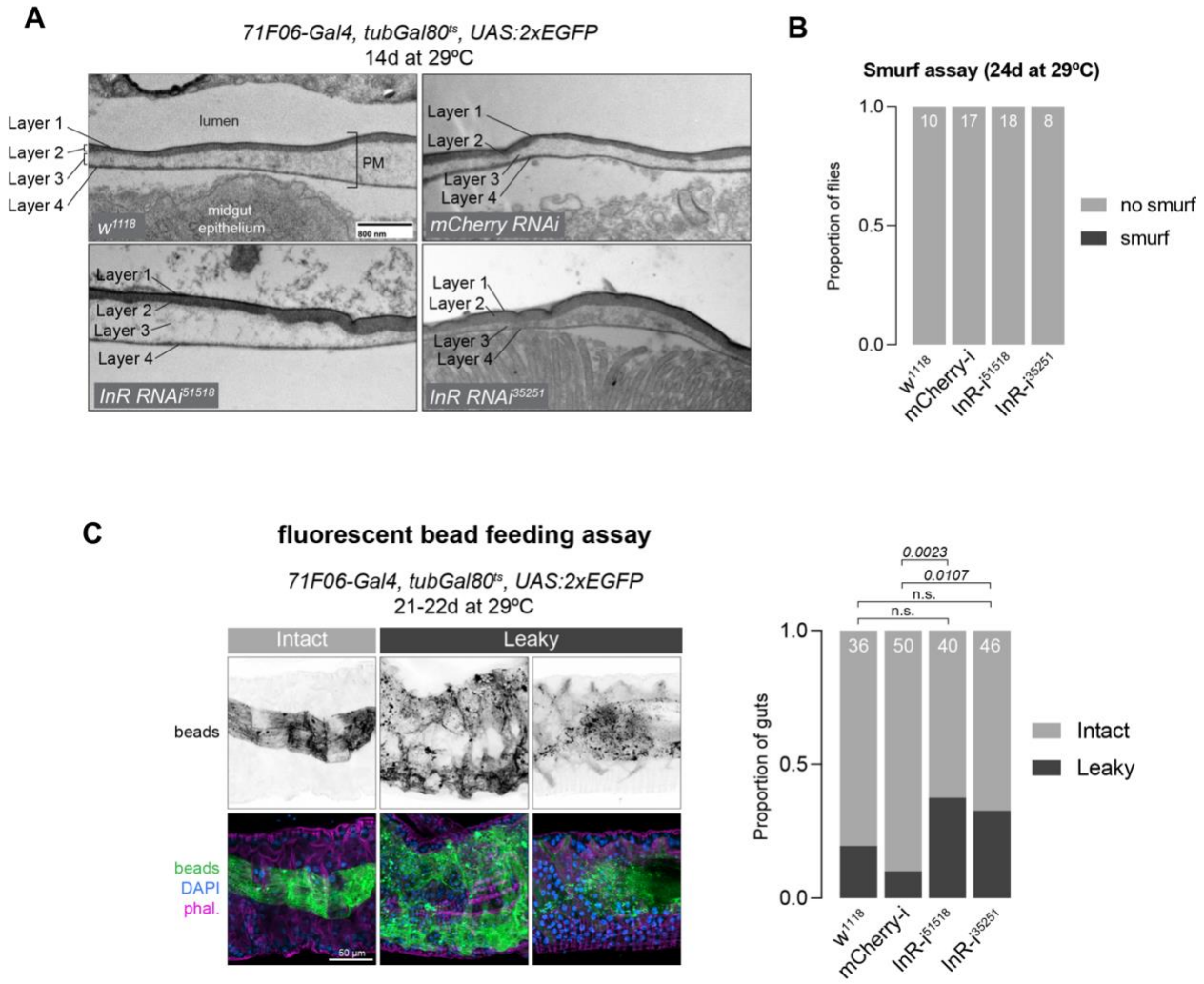

Supplementary Figure 11. Additional characterization of peritrophic membrane in *71F06^{ts} > InR-RNAi flies.* (A) Representative transmission electron microscopy images of peritrophic membrane in the anterior midgut of the indicated genotypes. The four-layered structure of the PM is visible in each case, with no gross morphological defects in *InR-RNAi* flies. (B) "Smurf" assay for leaky guts did not reveal any gut-defective flies after 24 days of RNAi expression. (C) Fluorescent bead retention assay. (Left) Examples of intact versus leaky guts that each sample was scored for. In intact guts, fluorescent beads were restricted to a "sleeve" of peritrophic membrane, whereas in "leaky" guts beads could be seen extending out to contact the gut epithelium. (Right) Quantification of leaky guts for each genotype. Three separate experiments were pooled, with total sample size given at the top of each column. Statistical tests are two-sided Fisher's Exact Test.

Supplementary Table 1: Genotypes used in this study

Figure	Genotype	Source Notes
1B, left	*yw ; + / wg[Sp-1] ; TI{GFP[3xP3.cLa]=CRIMIC.TG4.0}Chs2[CR60212-TG4.0] / P{w[+mC]=UAS-2xEGFP}AH3*	Chs2-Gal4: BL93534; UAS:2xEGFP: BL60293
1B, middle	*w ; P{w[+mC]=UAS-2xEGFP}AH2 ; P{w[+mW.hs]=GawB}Lk6[NP0101] / P{y[+t7.7] v[+t1.8]=VALIUM20-mCherry.RNAi}attP2*	"Cardia-Gal4": Kyoto DGRC 103522; UAS:2xEGFP: BL60292; mCherry RNAi: BL35785
1B, right	*w[1118] ; esg-Gal4, UAS:GFP, tubGal80[ts]*	Perrimon lab stock
1C, left	*w[1118] ; esg-Gal4, UAS:GFP, tubGal80[ts]*	Perrimon lab stock
1C right	*w[1118]; P{w[+mC]=10XStat92E-GFP}1*	Perrimon lab stock
1D	*Oregon R*	
1E	*Oregon R*	
1F,G	*w[1118] ; esg-Gal4, UAS:GFP, tubGal80[ts]*	Perrimon lab stock
2A	*w ; P{UAS-Stinger}2 / + ; P{y[+t7.7] w[+mC]=GMR71F06-GAL4}attP2 / MKRS*	UAS-Stinger: BL90920, GMR71F06-Gal4: BL39596
2E	*yw ; wg[Sp-1] / + ; Mi{Trojan-GAL4.0}Elovl7[MI01455-TG4.0] / P{w[+mC]=UAS-2xEGFP}AH3*	Elovl7-Gal4: BL67431
2E	*yw ; wg[Sp-1] / + ; TI{GFP[3xP3.cLa]=CRIMIC.TG4.2}CG11550[CR02741-TG4.2] / P{w[+mC]=UAS-2xEGFP}AH3*	CG11550-Gal4: BL97589
2E	*yw ; P{y[+t7.7] w[+mC]=Tub-GAL4.C-int}attP40 / + ; TI{RFP[3xP3.PB]=2A-GAL4(1-20)::N-int}Ppn[G4-N-int] / P{w[+mC]=UAS-2xEGFP}AH3*	Ppn-C-int: BL602730; tub-Gal4-C-int: BL602738
2E	*yw ; wg[Sp-1] / + ; TI{GFP[3xP3.cLa]=CRIMIC.TG4.2}Lgr1[CR01685-TG4.2] / P{w[+mC]=UAS-2xEGFP}AH3*	Lgr1-Gal4: BL86491
2E	*yw ; y[1] w[*]; Mi{Trojan-GAL4.2}Wnt4[MI03717-TG4.2] / wg[Sp-1] ; P{w[+mC]=UAS-2xEGFP}AH3*	Wnt4-Gal4: BL67449
2E	*yw ; TI{GFP[3xP3.cLa]=CRIMIC.TG4.2}Ca-Ma2d[CR01742-TG4.2] / wg[Sp-1] ; P{w[+mC]=UAS-2xEGFP}AH3*	Ca-Ma2d-Gal4: BL86499
2E	*w[*] TI{RFP[3xP3.PB]=2A-GAL4(1-20)::N-int}Mco4[G4-N-int] ; P{y[+t7.7] w[+mC]=Tub-GAL4.C-int}attP40 / + ; P{w[+mC]=UAS-2xEGFP}AH3 / +*	Mco4-N-int: BL605167; tub-Gal4-C-int: BL602738
2E	*yw ; wg[Sp-1] / + ; TI{GFP[3xP3.cLa]=CRIMIC.TG4.2}SecCl[CR01836-TG4.2]/TM3, Sb[1] Ser[1] / P{w[+mC]=UAS-2xEGFP}AH3*	SecCl-Gal4: BL91420
2E	*w ; Mex1-Gal4, UAS-2xEGFP*	Mex1-Gal4 gift of A. Petsakou (originally from Phillips & Thomas, 2006)

3A, left	*w ; P{w[+mC]=tubP-GAL80[ts]}10], P{w[+mC]=UAS-2xEGFP}AH2 ; P{y[+t7.7] w[+mC]=GMR71F06-GAL4}attP2*	GMR71F06-Gal4: BL39596, UAS:2xEGFP: BL60292, tubGal80ts: BL7108
3A, second to left	*w ; P{w[+mC]=tubP-GAL80[ts]}10], P{w[+mC]=UAS-2xEGFP}AH2 ; P{y[+t7.7] w[+mC]=GMR71F06-GAL4}attP2 / P{y[+t7.7] w[+mC]=UAS-yki.S111A.S168A.S250A.V5}attP2*	yki[3SA]: BL28817
3A, third to left	*w ; P{w[+mC]=tubP-GAL80[ts]}10], P{w[+mC]=UAS-2xEGFP}AH2 ; P{y[+t7.7] w[+mC]=GMR71F06-GAL4}attP2 / UAS:Ras[1A]*	Ras1A: gift of Chiwei Xu, Perrimon Lab
3A, fourth to left	*w ; P{w[+mC]=tubP-GAL80[ts]}10], P{w[+mC]=UAS-2xEGFP}AH2 ; P{y[+t7.7] w[+mC]=GMR71F06-GAL4}attP2*	
3A, right	*w ; P{w[+mC]=tubP-GAL80[ts]}10], P{w[+mC]=UAS-2xEGFP}AH2 ; P{y[+t7.7] w[+mC]=GMR71F06-GAL4}attP2 / P{y[+t7.7] v[+t1.8]=TRiP.HMS00001}attP2*	Notch-RNAi: BL33611
4	hsFLP, FRT19A, tubGal80 / P{ry[+t7.2]=neoFRT}19A; ry[506] ; ; tub-Gal4, UAS-GFP	FRT19A: BL1709; MARCM19A: Gift of P. Jouandin
5A, top	*w ; P{w[+mC]=UAS-rpr.C}14 / + ; P{w[+mC]=tubP-GAL80[ts]}ncd[GAL80ts-7] / +*	UAS-rpr: BL5824; tubGal80ts: BL7018
5A, bottom	*w ; P{w[+mC]=UAS-rpr.C}14 / TI{GFP[3xP3.cLa]=CRIMIC.TG4.2}Ca-Ma2d[CR01742-TG4.2] ; P{w[+mC]=tubP-GAL80[ts]}ncd[GAL80ts-7] / +*	Elovl7-Gal4: BL67431
5B, top	*w ; P{w[+mC]=UAS-rpr.C}14 / + ; P{w[+mC]=tubP-GAL80[ts]}ncd[GAL80ts-7] / +*	
5B, bottom	*w ; P{w[+mC]=UAS-rpr.C}14 / + ; P{w[+mC]=tubP-GAL80[ts]}ncd[GAL80ts-7] / TI{GFP[3xP3.cLa]=CRIMIC.TG4.2}CG11550[CR02741-TG4.2]*	CG11550-Gal4: BL97589
5C, top	*w ; P{w[+mC]=UAS-rpr.C}14 / + ; P{w[+mC]=tubP-GAL80[ts]}ncd[GAL80ts-7] / +*	
5C, bottom	*w ; P{w[+mC]=UAS-rpr.C}14 / + ; P{w[+mC]=tubP-GAL80[ts]}ncd[GAL80ts-7] / Mi{Trojan-GAL4.0}Elovl7[MI01455-TG4.0]*	Ca-Ma2d-Gal4: BL86499
6	*w ; P{UAS-Stinger}2 / + ; P{y[+t7.7] w[+mC]=GMR71F06-GAL4}attP2 / MKRS*	UAS-Stinger: BL90920, GMR71F06-Gal4: BL39596
7B, left	*w ; P{w[+mC]=UAS-rpr.C}14 / + ; P{w[+mC]=tubP-GAL80[ts]}ncd[GAL80ts-7] / +*	UAS-rpr: BL5824; tubGal80ts: BL7018
7B, right	*w ; P{w[+mC]=UAS-rpr.C}14 / + ; P{w[+mC]=tubP-GAL80[ts]}ncd[GAL80ts-7] / P{y[+t7.7] w[+mC]=GMR71F06-GAL4}attP2*	GMR71F06-Gal4: BL39596
7E	*OregonR*	

8A, left	*w ; P{w[+mC]=tubP-GAL80[ts]}10], P{w[+mC]=UAS-2xEGFP}AH2 ; P{y[+t7.7] w[+mC]=GMR71F06-GAL4}attP2 / +*	
8A, second to left	*w ; P{w[+mC]=tubP-GAL80[ts]}10], P{w[+mC]=UAS-2xEGFP}AH2 ; P{y[+t7.7] w[+mC]=GMR71F06-GAL4}attP2 / P{w[+mC]=UAS-CycE.L}ML1*	UAS-CycE: BL4781
8A, second to right	*w ; P{w[+mC]=tubP-GAL80[ts]}10], P{w[+mC]=UAS-2xEGFP}AH2 ; P{y[+t7.7] w[+mC]=GMR71F06-GAL4}attP2 / +*	
8A, right	*w ; P{w[+mC]=tubP-GAL80[ts]}10], P{w[+mC]=UAS-2xEGFP}AH2 ; P{y[+t7.7] w[+mC]=GMR71F06-GAL4}attP2 / M{w[+mC]=UAS-Myc.HA.WT}ZH-86Fb*	UAS-Myc: BL64759
8B, left	*w ; P{UAS-Stinger}2, P{w[+mC]=tubP-GAL80[ts]}10] / + ; P{y[+t7.7] w[+mC]=GMR71F06-GAL4}attP2 / +*	
8B, middle	*w ; P{UAS-Stinger}2, P{w[+mC]=tubP-GAL80[ts]}10] / + ; P{y[+t7.7] w[+mC]=GMR71F06-GAL4}attP2 / P{w[+mC]=UAS-CycE.L}ML1*	UAS-CycE: BL4781
8A, right	*w ; P{UAS-Stinger}2, P{w[+mC]=tubP-GAL80[ts]}10] / + ; P{y[+t7.7] w[+mC]=GMR71F06-GAL4}attP2 / M{w[+mC]=UAS-Myc.HA.WT}ZH-86Fb*	UAS-Myc: BL64759
8C, D, E left	*w ; P{w[+mC]=tubP-GAL80[ts]}10], P{w[+mC]=UAS-2xEGFP}AH2 ; P{y[+t7.7] w[+mC]=GMR71F06-GAL4}attP2 / +*	
8C, D, E middle	*w ; P{w[+mC]=tubP-GAL80[ts]}10], P{w[+mC]=UAS-2xEGFP}AH2 ; P{y[+t7.7] w[+mC]=GMR71F06-GAL4}attP2 / P{w[+mC]=UAS-CycE.L}ML1*	UAS-CycE: BL4781
8C, D, E right	*w ; P{w[+mC]=tubP-GAL80[ts]}10], P{w[+mC]=UAS-2xEGFP}AH2 ; P{y[+t7.7] w[+mC]=GMR71F06-GAL4}attP2 / M{w[+mC]=UAS-Myc.HA.WT}ZH-86Fb*	UAS-Myc: BL64759
9A, B	*w ; P{w[+mC]=tubP-GAL80[ts]}10], P{w[+mC]=UAS-2xEGFP}AH2 ; P{y[+t7.7] w[+mC]=GMR71F06-GAL4}attP2 / +*	
	w / y sc v sev; P{w[+mC]=tubP-GAL80[ts]}10], P{w[+mC]=UAS-2xEGFP}AH2 ; P{y[+t7.7] w[+mC]=GMR71F06-GAL4}attP2 / P{y[+t7.7] v[+t1.8]=VALIUM20-mCherry.RNAi}attP2	mCherry RNAi: BL35785
	w / y v ; P{w[+mC]=tubP-GAL80[ts]}10], P{w[+mC]=UAS-2xEGFP}AH2 / P{y[+t7.7] v[+t1.8]=TRiP.HMS03166}attP40 ; P{y[+t7.7] w[+mC]=GMR71F06-GAL4}attP2 / +	InR RNAi: BL51518
	w / y sc v sev; P{w[+mC]=tubP-GAL80[ts]}10], P{w[+mC]=UAS-2xEGFP}AH2 ; P{y[+t7.7] w[+mC]=GMR71F06-GAL4}attP2 / P{y[+t7.7] v[+t1.8]=TRiP.GL00139}attP2	InR RNAi: BL35251
9C	Same as 9A, except UAS-Stinger instead of UAS-2xEGFP	
9D-G	Same as 9A	
S1	*Oregon R*	
S2A, left	*w ; esg-Gal4, UAS:GFP, tubGal80[ts] ; +*	
S2A, right	*w ; esg-Gal4, UAS:GFP, tubGal80[ts] ; P{y[+t7.7] w[+mC]=UAS-yki.S111A.S168A.S250A.V5}attP2*	
S2C	*w ; esg-Gal4, UAS:GFP, tubGal80[ts] ; +*	

S2C	*w ; esg-Gal4, UAS:GFP, tubGal80[ts] ; UAS:Impl2*	UAS:ImpL2: Gift of Ying Liu
S2C	*w ; esg-Gal4, UAS:GFP, tubGal80[ts] / UAS:upd3 ; +*	UAS:upd3: Gift of Ying Liu
S2C	*w ; esg-Gal4, UAS:GFP, tubGal80[ts] / UAS:upd3 ; UAS:Impl2*	UAS:Impl2; UAS:upd3; Gift of A. Petsakou
S2D	*w ; dMef2-Gal4 / + ; tubGal80[ts] / +*	dMef2-Gal4: Perrimon Lab stock
S2D	*w ; dMef2-Gal4 / UAS:Impl2 ; tubGal80[ts] / +*	UAS:ImpL2: Gift of Ying Liu
S2D	*w ; dMef2-Gal4 / + ; tubGal80[ts] / UAS:upd3*	UAS:upd3: Gift of Ying Liu
S2D	*w ; dMef2-Gal4 / UAS:upd3 ; tubGal80[ts] / UAS:Impl2*	UAS:Impl2; UAS:upd3; Gift of A. Petsakou
S3	hsFLP, FRT19A, tubGal80 / P{ry[+t7.2]=neoFRT}19A; ry[506] ; ; tub-Gal4, UAS-GFP	FRT19A: BL7109; MARCM19A: Gift of P. Jouandin
S4A-E, left	*w ; P{w[+mC]=tubP-GAL80[ts]}10], P{w[+mC]=UAS-2xEGFP}AH2 ; P{y[+t7.7] w[+mC]=GMR71F06-GAL4}attP2*	GMR71F06-Gal4: BL39596, UAS:2xEGFP: BL60292, tubGal80ts: BL7108
S4A-E, middle	*w ; P{w[+mC]=tubP-GAL80[ts]}10], P{w[+mC]=UAS-2xEGFP}AH2 ; P{y[+t7.7] w[+mC]=GMR71F06-GAL4}attP2 / P{y[+t7.7] w[+mC]=UAS-yki.S111A.S168A.S250A.V5}attP2*	yki[3SA]: BL28817
S4A-E, right	*w ; P{w[+mC]=tubP-GAL80[ts]}10], P{w[+mC]=UAS-2xEGFP}AH2 ; P{y[+t7.7] w[+mC]=GMR71F06-GAL4}attP2 / Ras[1A]*	Ras1A: gift of Chiwei Xu, Perrimon Lab
S4F-I, left	*w ; P{w[+mC]=tubP-GAL80[ts]}10], P{w[+mC]=UAS-2xEGFP}AH2 ; P{y[+t7.7] w[+mC]=GMR71F06-GAL4}attP2*	
S4F-I, middle	*w ; P{w[+mC]=tubP-GAL80[ts]}10], P{w[+mC]=UAS-2xEGFP}AH2 ; P{y[+t7.7] w[+mC]=GMR71F06-GAL4}attP2 / P{y[+t7.7] v[+t1.8]=VALIUM20-mCherry.RNAi}attP2*	mCherry RNAi: BL35785
S4F-I, right	*w ; P{w[+mC]=tubP-GAL80[ts]}10], P{w[+mC]=UAS-2xEGFP}AH2 ; P{y[+t7.7] w[+mC]=GMR71F06-GAL4}attP2 / P{y[+t7.7] v[+t1.8]=TRiP.HMS00001}attP2*	Notch-RNAi: BL33611
S5	hsFLP, FRT19A, tubGal80 / P{ry[+t7.2]=neoFRT}19A; ry[506] ; ; tub-Gal4, UAS-GFP	FRT19A: BL1709; MARCM19A: Gift of P. Jouandin
S6A, left	*w ; P{y[+t7.7] w[+mC]=GMR71F06-GAL4.C-int}attP40 / P{w[+mC]=UAS-2xEGFP}AH2 ; P{y[+t7.7] w[+mC]=Tub-GAL4.C-int}attP2*	GMR71F06-Gal4-C-int: This manuscript

S6A, middle	*w ; P{y[+t7.7] w[+mC]=Tub-GAL4.C-int}attP40 ; TI{RFP[3xP3.PB]=2A-GAL4(1-20)::N-int}Delta[G4-N-int] / P{w[+mC]=UAS-2xEGFP}AH3*	Delta-Gal4-N-int: BL602717
S6A, right	*w ; P{y[+t7.7] w[+mC]=GMR71F06-GAL4.C-int}attP40 / P{w[+mC]=UAS-2xEGFP}AH2 ; TI{RFP[3xP3.PB]=2A-GAL4(1-20)::N-int}Delta[G4-N-int]*	
S6B	*w ; P{y[+t7.7] w[+mC]=GMR71F06-GAL4.C-int}attP40 / P{w[+mC]=UAS-2xEGFP}AH2 ; TI{RFP[3xP3.PB]=2A-GAL4(1-20)::N-int}Delta[G4-N-int]*	
S6C	*w ; P{y[+t7.7] w[+mC]=GMR71F06-GAL4.C-int}attP40 / w ; P{y[+t7.7] w[+mC]=GMR71F06-GAL4.C-int}attP40 / P{w[+mC]=UAS-2xEGFP}AH2 ; TI{RFP[3xP3.PB]=2A-GAL4(1-20)::N-int}Delta[G4-N-int] ; TI{RFP[3xP3.PB]=2A-GAL4(1-20)::N-int}Delta[G4-N-int] / P{w[+mC]=tubP-GAL80[ts]}ncd[GAL80ts-7]*	GTRACE: BL28280
S7	*w ; P{UAS-Stinger}2 / + ; P{y[+t7.7] w[+mC]=GMR71F06-GAL4}attP2 / MKRS*	UAS-Stinger: BL90920, GMR71F06-Gal4: BL39596
S8	*w ; P{UAS-Stinger}2 / + ; P{y[+t7.7] w[+mC]=GMR71F06-GAL4}attP2 / MKRS*	UAS-Stinger: BL90920, GMR71F06-Gal4: BL39596
S9	See Figure 8.	
S10A, left	*w ; P{w[+mC]=tubP-GAL80[ts]}10], P{UAS-Stinger}2 ; P{y[+t7.7] w[+mC]=GMR71F06-GAL4}attP2 / +*	
S10A, middle	*w / y sc v sev ; P{w[+mC]=tubP-GAL80[ts]}10], P{UAS-Stinger}2 ; P{y[+t7.7] w[+mC]=GMR71F06-GAL4}attP2 / P{y[+t7.7] v[+t1.8]=VALIUM20-mCherry.RNAi}attP2*	mCherry RNAi: BL35785
S10A, right	*w ; P{w[+mC]=tubP-GAL80[ts]}10], P{UAS-Stinger}2 / fzr RNAi GD25550 ; P{y[+t7.7] w[+mC]=GMR71F06-GAL4}attP2*	fzr RNAi: VDRC GD-25550
S10B, left	*w ; P{w[+mC]=tubP-GAL80[ts]}10], P{UAS-Stinger}2 ; P{y[+t7.7] w[+mC]=GMR71F06-GAL4}attP2 / +*	
S10B, middle	*w / y sc v sev; P{w[+mC]=tubP-GAL80[ts]}10], P{UAS-Stinger}2 ; P{y[+t7.7] w[+mC]=GMR71F06-GAL4}attP2 / P{y[+t7.7] v[+t1.8]=VALIUM20-mCherry.RNAi}attP2*	mCherry RNAi: BL35785
S10B, right	*w / y sc v sev ; P{w[+mC]=tubP-GAL80[ts]}10], P{UAS-Stinger}2 / + ; P{y[+t7.7] w[+mC]=GMR71F06-GAL4}attP2 / P{y[+t7.7] v[+t1.8]=TRiP.HMS01541}attP2*	E2F1 RNAi: BL36136
S10C, left	*w ; P{w[+mC]=tubP-GAL80[ts]}10], P{w[+mC]=UAS-2xEGFP}AH2 ; P{y[+t7.7] w[+mC]=GMR71F06-GAL4}attP2 / +*	
S10C, middle	*w / y sc v sev; P{w[+mC]=tubP-GAL80[ts]}10], P{w[+mC]=UAS-2xEGFP}AH2 ; P{y[+t7.7] w[+mC]=GMR71F06-GAL4}attP2 / P{y[+t7.7] v[+t1.8]=VALIUM20-mCherry.RNAi}attP2*	mCherry RNAi: BL35785
S10C, right	*w / y y sc v sev; P{w[+mC]=tubP-GAL80[ts]}10], P{w[+mC]=UAS-2xEGFP}AH2 ; P{y[+t7.7] w[+mC]=GMR71F06-GAL4}attP2 / P{y[+t7.7] v[+t1.8]=TRiP.HMS01538}attP2*	myc RNAi: BL36123

S10D-G, left	*w ; P{w[+mC]=tubP-GAL80[ts]}10], P{w[+mC]=UAS-2xEGFP}AH2 ; P{y[+t7.7] w[+mC]=GMR71F06-GAL4}attP2 / +*	
S10D-G, middle	*w / y sc v sev ; P{w[+mC]=tubP-GAL80[ts]}10], P{w[+mC]=UAS-2xEGFP}AH2 ; P{y[+t7.7] w[+mC]=GMR71F06-GAL4}attP2 / P{y[+t7.7] v[+t1.8]=VALIUM20-mCherry.RNAi}attP2*	mCherry RNAi: BL35785
S10D-G, right	*w / y v ; P{w[+mC]=tubP-GAL80[ts]}10], P{w[+mC]=UAS-2xEGFP}AH2 ; P{y[+t7.7] w[+mC]=GMR71F06-GAL4}attP2 / P{y[+t7.7] v[+t1.8]=TRiP.JF02473}attP2*	cycE RNAi: BL29314
S11	Same as 9A	